Nicolas Legrain

Landscape Evolution of the Eastern Alps

A Morphometric and Geochronological Study

A dissertation submitted to the

Faculty of Natural Science

Karl-Franzens University of Graz

Austria

August 2013

Abstract

The topographic evolution of the European Alps and its relationship with climate and tectonics remains strongly debated and relatively unconstrained. In this thesis, I investigate the long-term landscape evolution and its link with tectonic processes in a region of the Alps that has escaped glacial erosion during the last periodic glaciations: the easternmost end of the Alps. Morphometric analysis reveals the presence of incised relict landscapes in the Pohorje and Koralpe mountains and channel profiles projection shows that the amount of incision into these relict landscapes is 387 ± 105 m. Topographic analysis also shows that the relict landscape is present on both sides Koralpe block which has been considered to be tilted. The data presented here suggests that the relict landscape is younger than the tilting which probably took place between 18 Ma and 16 Ma. Apatite (U-Th)/He ages indicate that the Pohorje granite had cooled down below the closure temperature of 70°C by 15 Ma. As the Pohorje relict landscape is developed across the contacts of Pohorje granite, it implies that this relict landscape must be younger than 15 Ma. Taken together, these results suggest that both the Koralpe and Pohorje relict landscapes have formed between 16-15 Ma and 5 Ma, a period of tectonic quiescence that lead to decay and smoothing of the topography. ^{10}Be-derived erosion rates from the Koralpe Mountain average 49 ± 8 m/Ma for catchments located on the relict landscape, above the knickpoints, and 137 ± 15 m/Ma for catchments in the incised landscape, below the knickpoints. This significant difference in erosion rate between relict and incised landscape strongly support the interpretation of the Koralpe landscape as a transient landscape experiencing a wave of incision. I calculate an estimation for the onset of incision at 4 ± 1 Ma, an estimation of surface uplift of 349 ± 92 m, and a total relative base level fall of 543 ± 143 m. The results are in close agreement with both the magnitude and the age of onset of uplift of the Styrian Basin and the North Molasse Basin, as well as the incision rate of the Mur River into the Styrian Karst. We suggest that the whole area is experiencing the same post-Miocene increased rock uplift rate, possibly in response to a deep-seated process such as delamination of the lithosphere below the Alps or a slab break-off.

Outline of the thesis

This thesis is divided into three chapters and one appendix.

In **Chapter 1**, a combination of morphometric analysis and apatite (U-Th)/He thermochronology is used to study the topographic evolution of the Koralpe and Pohorje Mountains located at the southeastern end of the Alps. This chapter is currently under review in *Geomorphology*:

- **Legrain, N., Stüwe, K., Wölfler, A.,** 2013. Incised relict landscapes in a never glaciated part of the Eastern Alps.

In **Chapter 2,** the incision into the Koralpe relict landscape is quantified by cosmogenic ^{10}Be-derived erosion rates of the different part of the Koralpe landscape. This chapter is currently under review in *Earth Surface Processes and Landforms*:

- **Legrain, N., Dixon, J.L., Stüwe, K., von Blanckenburg, F., Kubik, P.,** 2013. Landscape rejuvenation and post-Miocene increase in rock uplift rate at the eastern end of the Alps.

Chapter 3 contains the overall conclusions and outlook of this thesis.

In **Appendix** is a collection of abstract from different conferences where I contributed to during this PhD.

- **Wölfler, A., Legrain, N., Stüwe, K., Fritz, H.**, 2009. 4D kinematics of the Neogene Eastern Alps: An ArcGis based analysis of horizontal and vertical kinematics, 9th Workshop on Alpine Geological Studies, Cogne, Italy.

- **Stüwe, K., Wagner, T., Wölfler, A., Legrain, N.**, 2009. Active tectonics at the Eastern end of the Alps: The Alps are certainly not “dead” at all, Geophysical Research Abstracts 11, EGU2009-9332, EGU General Assembly, Vienna, Austria.

- **Legrain, N., Stüwe, K.,** 2010. Evidence of young regional uplift in the non-glaciated Easternmost Alps: the dissected relict landscape of the Styrian margins, Journal of Alpine Geology 52, Leoben, Austria.

- **Stüwe, K., Legrain, N.**, **Hergarten, S.,** 2010. Mapping out Paleo-Landscapes in the Non-Glaciated Part of the Alps: More Evidence for Young Uplift of this Part of the Alps. Geophysical Research Abstracts 12, EGU2010-11297, EGU General Assembly, Vienna, Austria.

- **Wölfler, A., Stüwe, K., Legrain, N., Fritz, H.,** 2010. Late Neogene denudation rates in the Eastern Alps as determined by low temperature thermochronology, Journal of Alpine Geology 52, Leoben, Austria.

- **Wölfler, A., Stüwe, K., Legrain, N., Fritz, H.,** 2011. Neogene denudation rates in the Eastern Alps as determined by low temperature thermochronology, Geophysical Research Abstracts 13, EGU2011-10101, EGU General Assembly, Vienna, Austria.

- **Stüwe, K., Legrain, N., Wölfler, A., Dunkl, I., Ehlers, T.**, 2011. New U-He ages from the Eastern Alps, Geophysical Research Abstracts 13, EGU2011-8617, EGU General Assembly, Vienna, Austria.

- **Stüwe, K., Legrain, N., Wölfler, A., Wagner, T., Hergarten, S.**, 2011. Young Uplift at the Eastern end of the Alps: Evidence and tectonic implications for the Alps-Pannonian Basin transition zone, Geological/Geophysical Meeting, Sopron, Hungary.

- **Legrain, N., Stüwe, K., Dixon, J.L., von Blanckenburg, F., Kubik, P.**, 2011. Large scale, small amplitude, post-Miocene surface uplift in the non-glaciated Eastern Alps: river profiles analysis and cosmogenic-derived ^{10}Be denudation rates, Geophysical Research Abstracts 13, EGU2011-10708, EGU General Assembly, Vienna, Austria.

Contents

Chapter 1

Incised Relict Landscapes in a Never Glaciated Part of the Eastern Alps

Abstract

We investigate long-term landscape evolution and its link with tectonic processes, in a region of the Alps that has escaped glacial erosion during the last periodic glaciations: the easternmost end of the Alps. Morphometric analysis reveals the presence of incised relict landscapes in the Pohorje and Koralpe mountains and channel profiles projection shows that the amount of incision into these relict landscapes is 387 ± 105 m. This incision likely occurred during the last 6-5 Ma in response to uplift of the whole region, by analogy with subsidence analysis of the Styrian Basin. Topographic analysis also shows that the relict landscape is present on both sides of the eastward tilted Koralpe block. This suggests that the relict landscape is younger than the tilting which probably took place between 18 Ma and 16 Ma. We also use apatite (U-Th)/He thermochrono-logy to constrain the possible age of the Koralpe and Pohorje relict landscapes. They indicate that the Pohorje granite had cooled down below the closure temperature of 70°C by 15 Ma. As the Pohorje relict landscape is developed onto and cross-cut the granite, it implies that this relict landscape must be, at least, younger than 15 Ma. These results suggest that both relict landscapes have formed between 16-15 Ma and 5 Ma, a period of tectonic quiescence that lead to decay and smoothing of the topography, before the ~ 400 m incision of the Koralpe and Pohorje landscapes that took place since the late Miocene.

1.1. Introduction

Topography is the result of a competition between erosion that removes material from the Earth's surface, and tectonic forces that can create relief through uplift mechanisms. However, tectonics, climate and topography are linked by complex interactions and feedback mechanisms. In order to improve our understanding of these processes, quantifying the topographic evolution of mountain ranges is very important. In the European Alps, the debate on the landscape evolution and its relationship with tectonics and climate remains ongoing (Cederbom et al., 2004; Persaud and Pfiffner, 2004; Champagnac et al., 2007; Willett, 2010; Hergarten et al., 2010; Norton et al., 2010, Valla et al., 2011, Sternai et al., 2012). Here we infer aspects of the long-term landscape evolution of the Alps by focusing on a part of the Eastern Alps that was free of ice during the last periodic glaciations (van Husen, 1997), but features a mountainous landscape with summits up to 2200 m high elevation: the easternmost part of the Eastern Alps (Fig. 1.1).

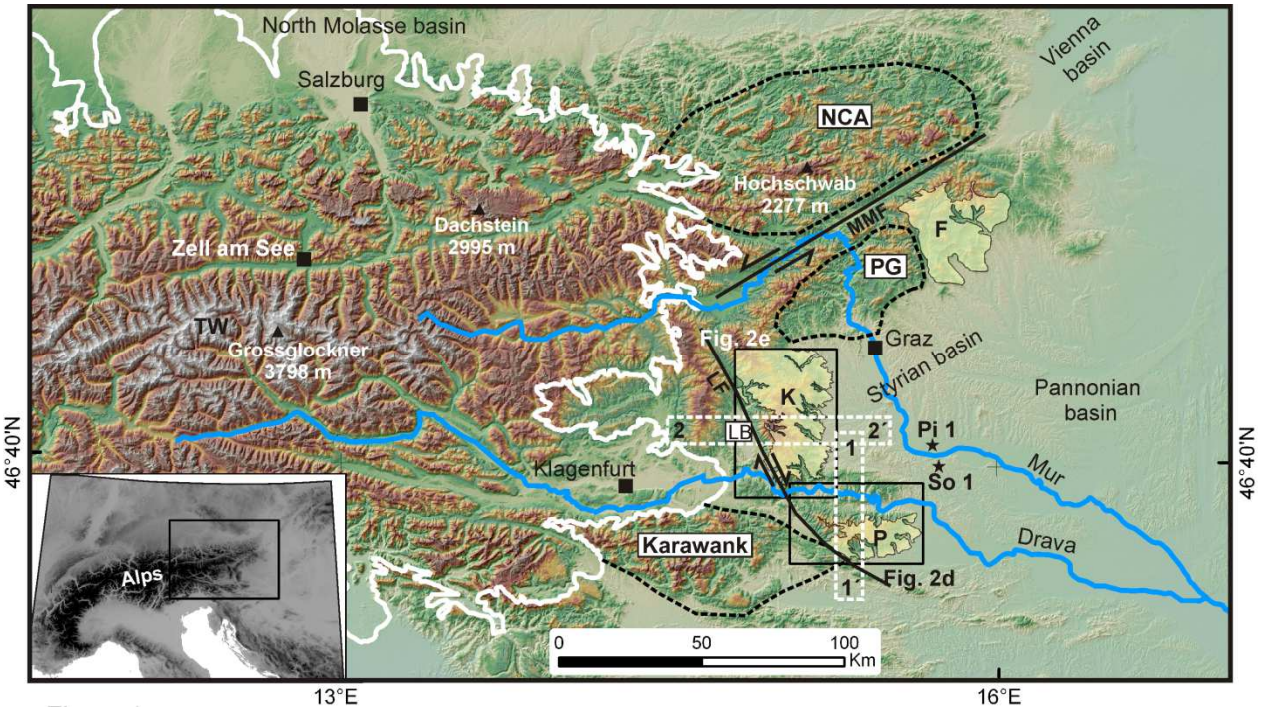

Figure 1.1: Topography of the easternmost part of the European Alps and location of the studied areas. Relict landscapes are yellow polygons, thick white line represents LGM glacier boundary. NCA: Northern Calcareous Alps; TW: Tauern window; PG: Paleozoic of Graz; K: Koralpe relict landscape; P: Pohorje relict landscape; LB: Lavanttal Basin; LF: Lavanttal fault; MMF: Mur-Mürz fault. F refers to the Fischbacher Mountain that possibly represents an incised relict landscape. Location of wells for subsidence analysis: So 1: Somat 1; Pi 1: Pichla 1 (Ebner and Sachsenhofer, 1995; Sachsenhofer et al., 1998; 2001).White dashed rectangles are extent of swath profiles of Fig. 1.4 (profiles 1-1´ and 2-2´).

As this region was not affected by glacial carving, this landscape represents a unique opportunity to study morphometric parameters to document the long-term (Ma timescale) landscape evolution of the area.

Paleosurfaces or relict landscapes have long been documented in the studied area, in particular for the Koralpe Mountain. Indeed, Winkler-Hermaden (1957) already suggested that the Koralpe Mountain features preserved ´paleosurfaces´ or relict landscapes as we term these landforms in this article. More recently, the Koralpe landscape has been considered as an Oligocene paleosurface by Frisch et al. (2000). Robl et al. (2008) have also suspected that knickpoints may be recorded in the river profiles of some of the tributaries of the Drava and the Mur draining the Koralpe and Pohorje mountains, possibly indicating transient erosion. However, the Koralpe and Pohorje landforms were never mapped by using quantitative methods and Digital Elevation Models (DEM) and the age of their formation and incision remains largely unconstrained. To investigate the landscape evolution, the uplift history and the links with tectonic events in this part of the Alps, we analyze channel profiles and slope maps to present maps of incised relict landscapes for the Koralpe and Pohorje Mountains. Then, we use channel profile projection of eight selected rivers to estimate the amount of incision into these relict landscapes. We combine our results with 20 new apatite (U-Th)/He ages (AHe) from the Koralpe and Pohorje mountains that we use to constrain our interpretations in absolute time. Finally, we infer an integrated landscape evolution scenario for the studied area, in a never glaciated part of the Eastern Alps, linking tectonic and landscape evolution of the region since the Early Miocene.

1.2. Geological setting

The Pohorje Massif and the Koralpe region are both part of what has been termed the Styrian Block east of the Lavanttal fault system and south of the Mur-Mürz system (Fig. 1.1) (Wagner et al., 2011). The Lavanttal fault system and the Mur-Mürz systems are both some of the major structures controlling the Miocene lateral extrusion of the Eastern Alps (Ratschbacher et al., 1991, Frisch et al., 1998; Robl and Stüwe, 2005, Wölfler et al., 2010; 2011) and are therefore closely linked to the tectonic evolution of the region (Fig. 1.1). The regional base level for the entire eastern end of the Alps is set by the Danube which ultimately drains into the Black Sea. More locally, the current base levels for the region under investigation are the

Drava and the Mur rivers (Fig. 1.1). These two major rivers seem to be morphologically well-equilibrated and do not record significant knickpoints other than the ones located at the LGM terminal moraines (Robl et al., 2008). The Styrian basin consists of sediments that were deposited between approximately 18 Ma and 7 Ma (Ebner and Sachsenhofer, 1995). This region is characterized by a smooth hilly landscape and extensive alluvial plains and fluvial terraces (e.g. Wagner et al., 2011).

The Pohorje Massif lies at the southeastern corner of the Alps (1.1). The massif is about 35 km long and 15 km wide and it is surrounded by the westernmost parts of the Pannonian basin to the south and to the east. The elevation of the Miocene basin to the south is about 300 m and the highest summit of Pohorje is Črni Vrh with an elevation of 1543 m. The massif is made up of eclogite facies Cretaceous paragneisses of the Austroalpine nappe complex. The metamorphic rocks of the Pohorje Mountain were intruded by the Pohorje pluton, a 30 km long and 4-8 km wide magmatic body (Fig. 1.2d). U-Pb analysis on zircons imply an Early Miocene crystallization age of the granite and zircon fission track ages indicate rapid cooling of the pluton within about 3 million years (Fodor et al., 2008). However, cooling and exhumation of Pohorje pluton below about 250°C is currently unconstrained. It is known however, that the Pohorje pluton supplyed sediments into the Ribnica Trough in the centre of the massif already in the Middle Miocene. This is indicated by nearly synsedimentary detrital apatite cooling ages (Sachsenhofer et al., 1997; 1998; Dunkl et al., 2005). This is supported by kinematic data from east-west striking high-angle normal faults along the margin of the Ribnica Trough (Pischinger et al., 2008). Associated volcanic rocks at the western end of the massif and the thermochronological study by Fodor et al. (2008) indicate that the pluton cooled near the surface and that its exhumation during the early Miocene was very fast. Sölva et al. (2005) have noted that the course of the Drava River, that dissects the massif, indicates an antecedent river profile with young uplift of the massif.

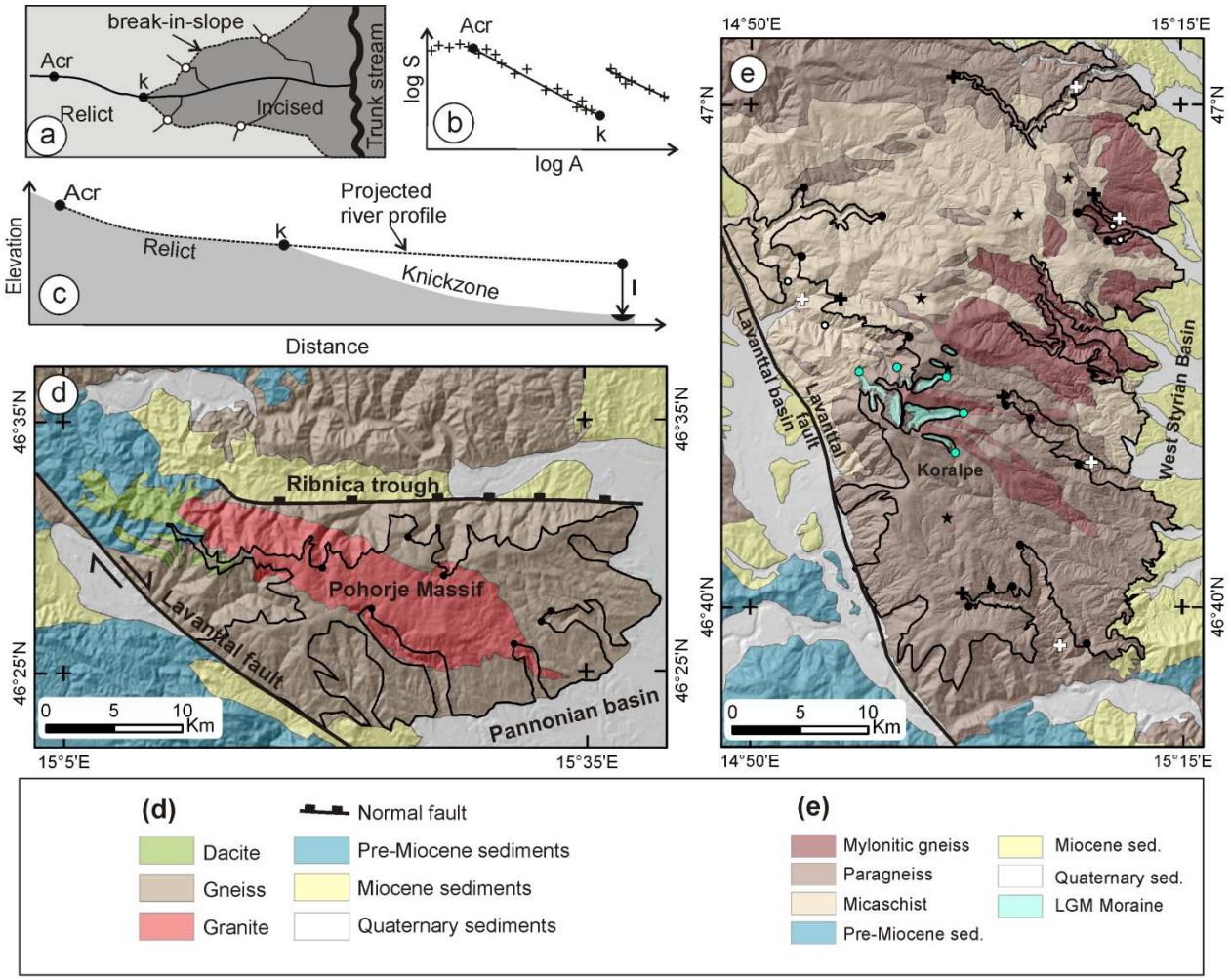

Figure 1.2: Method for mapping incised relict landscape and projecting channel profiles. (a) Map view of a relict and incised landscape, white points are location of knickpoints of tributaries; Points along river are: *Acr*: critical drainage area above which log (*S*) and log (*A*) start to be correlated; *k*: knickpoint. (b) Double logarithmic slope-area plot with fitted relict and knickzone segments; *S*: gradient in m/m; *A*: Drainage area in m². (c) River profile with the downstream projected relict river segment; *I* is incision calculated at the confluence with the trunk stream. For the rivers draining to Miocene basins, the incision was calculated at the transition between crystalline basement and basin. (d) Map of the Pohorje Mountain showing the extent of the relict landscape (black line) and lithology. (e) Map of the Koralpe Mountain, showing the mapped relict landscape (black line) and the lithology, for more details on other symbols refer to Fig. 1.3.

The Koralpe region is a north-south striking range located between the Styrian Basin to the east and the Miocene Lavanttal fault to the west (Fig. 1.1, 1.2e). The range measures ~40 km from north to south and ~25 km from east to west. It has an asymmetric topography from 2140 m on the Speikkogel summit to 300 m near the Styrian Basin, with a steep western slope and a gentle eastern slope, probably due to tilting of the range in response to the lateral extrusion of the Eastern Alps and the Early Miocene fault activity of the Lavanttal fault (Neubauer and Genser, 1990, Kurz et al., 2011). Lithologically, the range is famous for hosting the eclogite type locality and is one of the highest grade metamorphic regions of the Alps. It is made up of Cretaceous gneisses, amphibolites and eclogites. The Miocene Lavanttal fault system bounding the range to the west is part of the Pöls-Lavanttal fault

system (Fig. 1.2e) that has a dextral offset (Exner, 1976; Wölfer et al., 2010, 2011). In the Lavanttal segment, a small pull-apart basin shows evidence for about 15 km of dextral offset (Reischenbacher et al., 2007). Vertical offset along the Lavanttal fault system is estimated to be > 2 km, with relative upward movement of the Koralpe (Frisch et al., 2000). Onset of sedimentation in the Lavanttal Basin is dated at ~18 Ma (Strauss et al., 2001; Reischenbacher et al., 2007). Based on the sedimentary evolution of the Lavanttal Basin, the Lavanttal fault system is assumed to be active since the Early Miocene with peaks in activity at 18–16 and 14–12 Ma. Fault plane solutions for recent seismicity display clear dextral strike-slip movements (Reinecker and Lenhardt, 1999; Pischinger et al., 2008). The Koralpe Mountain was partly covered by small glaciers during the recent glaciation periods. These glaciers have left small cirques around the highest peaks, but the glaciers only covered and modified a very small part of the Koralpe landscape (Fig. 1.2d) that we exclude from the relict landscape mapping.

1.3. Methods

1.3.1. Mapping of incised and relict landscape

As we use the terms “relict” and “incised” landscapes in this study, is important to define these terms. Here we use the term “relict landscape” and “incised landscape” in their most simple definitions. It refers to the concept of an incision of rivers into a pre-existing morphology resulting in two different landscapes: the pre-existing “relict” landscape and the more recent “incised” landscape (Clark et al., 2006). The morphometric analysis was performed by using the SRTM3 digital elevation model (DEM). Although a 30 m resolution DEM exists (ASTER 30 m), a recent study suggests that, at the moment, the available version of the 30 m DEM is less accurate than the 90 m SRTM (Hirt et al., 2010) which was confirmed by a preliminary comparison of the two DEMs for some of the studied rivers. Channels were studied by using the empirical relationship between drainage area A and slope S of an equilibrated channel (Hack, 1973; Flint, 1974):

$$S = k_s A^{-\theta} \tag{1.1}$$

where θ and k_s are generally referred to as the concavity index and the channel steepness index, respectively (Wobus et al., 2006).

The data for A and S were extracted from the DEM by using the methods of Wobus et al. (2006) and the freely available Stream Profiler codes (Whipple et al., 2007). Because k_s is

strongly related to θ, a normalized channel steepness index (k_{sn}) is often calculated using a fixed reference concavity index (θ_{ref}). This allows for easier comparison between different channels or different channel segments. If the channel is considered to be in equilibrium, only single values of θ and k_s should be fitted in a doubly logarithmic slope-area plot (Fig. 1.2). Then, k_{sn} can be used as a proxy to infer information on rock uplift rates (Wobus et al., 2006). This can be illustrated by listing another definition of the steepness index where:

$$k_s = (U/K)^{1/n} \tag{1.2}$$

and U is the uplift rate and K and n are constants related to the material properties. The two equations above can be related and the interested reader is referred to Wobus et al. (2006) for their relationship.

If the channel is not in equilibrium, channel profiles will depart from the shape implied by the equations above. Thus, these relationships can also be used to identify different segments of the river profiles (Fig. 1.2). Then, the fit must be done separately for the different segments of the channel. Here we use this latter approach as all channel profiles presented here have marked knickzones, defined as a steep channel segment bound by less steep channel reaches. The uppermost point of the knickzone is defined as a knickpoint *k*. Interpretation of knickpoints or knickzones is not trivial as they may be controlled by either lithological boundaries or tectonic and climatic controls. As our interest is predominantly in tectonically and climatically related knickpoints, we have carefully compared the location of knickzones with lithological maps. Maps of normalized channel steepness index were calculated using a reference concavity index $\theta_{ref} = 0.45$ which is the most commonly used value in the literature (Fig. 1.3 a,c; Wobus et al., 2006). This allows for easier direct comparison with recent studies. Note that the choice of θ_{ref} does not change the relative pattern of k_{sn}.

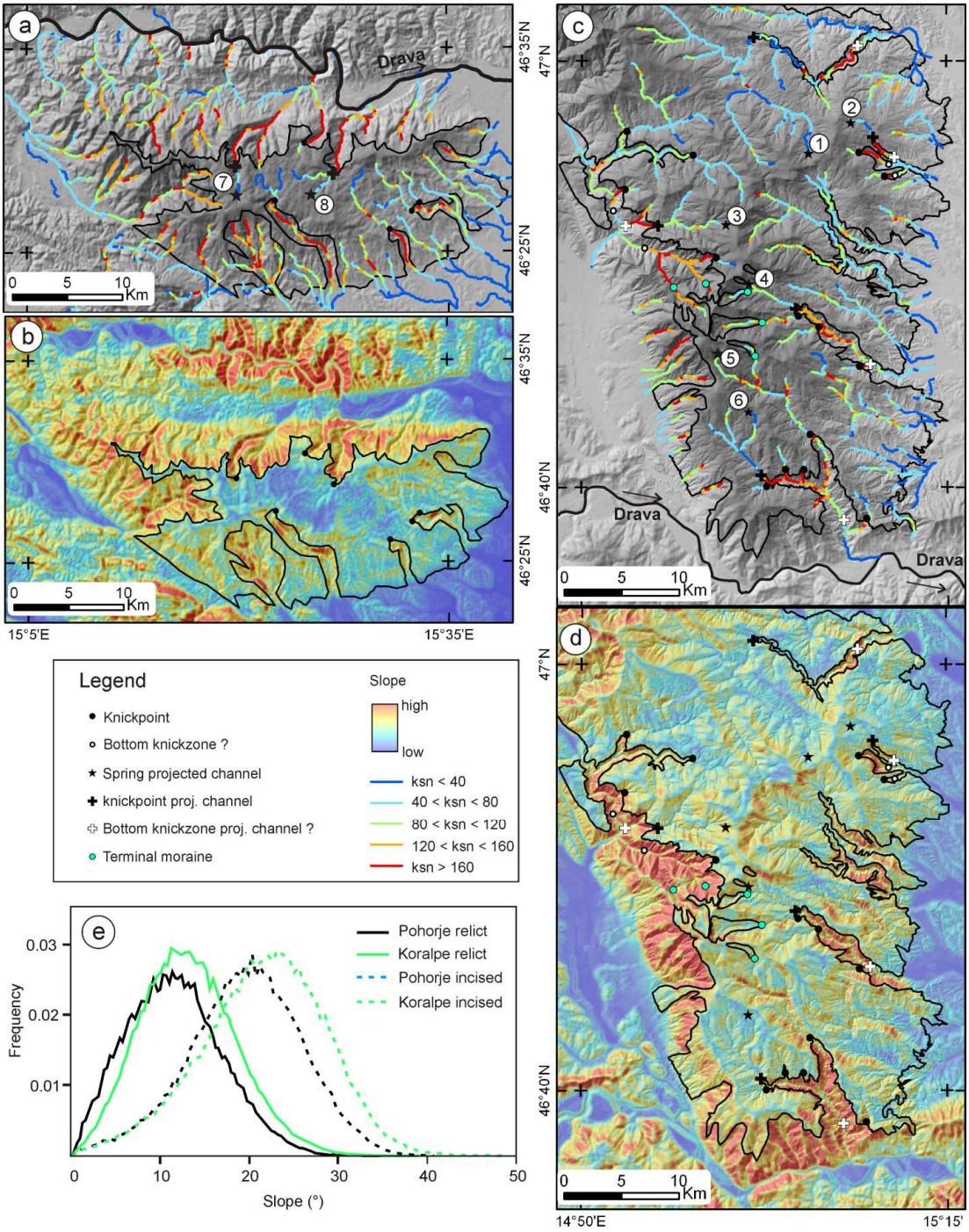

Figure 1.3: Mapping results for the Pohorje Massif, north Slovenia and Koralpe region, (a) Map of normalized channel steepness index (k_{sn}) for Pohorje, calculated with a reference concavity index of 0.45 and with 500 m segments along all channels with $A > 10^6$ m². Black line is the contour of the mapped relict landscape. Numbers refer to the projected channel profiles (b) Slope map of Pohorje, calculated from the 90 m SRTM data. Black line is the contour of the mapped relict landscape. (c) Map of normalized channel steepness index (k_{sn}) for Koralpe, calculated with a reference concavity index of 0.45 and with 500 m segments along all channels with $A > 10^6$ m². Black line is the contour of the mapped relict landscape. Numbers refer to the projected channel profiles. (d) Slope map of Koralpe, calculated from the 90 m SRTM data. Black line is the contour of the mapped relict landscape. The LGM small glacier are excluded from the relict landscape (see also Fig. 1.2) (e) Slope distribution of the Koralpe and Pohorje relict and incised landscapes. The slope distribution of the Pohorje and Koralpe relict landscapes are very similar as well as the slope distribution of the two incised landscapes.

We have mapped the incised valleys by following obvious breaks-in-slope based on the slope maps and the k_{sn} maps (Fig. 1.2, 1.3). The incised landscape is recognized by significantly higher slope and higher k_{sn} values than the surrounding relict landscape (Fig. 1.3a). The mapping of relict and incised landscape was based on the DEM analysis and cross-checked with field observations. Field work consisted in comparing the bedrock versus alluvial parts of the channels as well as the soil thickness in the incised part of the landscape and on the relict landscape. Bedrock or mixed bedrock-alluvial channels in the incised parts of a landscape are a good indication of relatively active incision, while alluvial channels were often observed in the relict landscape and indicate a rather low channel erosion process.

1.3.2. Channel profiles projection

The amount of incision into a relict landscape can be estimated by projecting "relict" river segments (Schoenbohm et al., 2004; Clark et al., 2005). This method commonly uses a fixed reference concavity index (θ_{ref}) to calculate the steepness index and then extrapolate the relict channel profile downstream. The amount of incision is taken as the vertical difference between the extrapolated and the present day channel profile (Fig. 1.2). The reference concavity index is usually taken as the average value of the concavity indices observed in the relict river segments from a sufficient number of rivers. This approach is thus relevant for studying large areas where many channels are present. Here, only approximately 20 main rivers are present for the Koralpe and Pohorje mountains because the studied region is small. Of these 20 channels, 8 were found to be suitable for downstream projection. For the other channels, the incision wave has migrated to far upstream and the remaining relict segment is too small to be reliably projected downstream and. Our choice of only 8 rivers on approximately 20 does not however bring into doubt the interpretation of an incised relict landscape for the entire Pohorje and Koralpe mountains, as it can be clearly seen at the scale of the entire area on Fig. 1.3. To ensure a reliable and unambiguous downstream projection, the 8 channels were chosen based on conservative arguments on the robustness of their fit in the slope-area plots.

We have thus used θ and k_s values given by the best fit of the relict river segment of each individual river (Fig. 1.2). The relict river segment was defined between a minimum critical drainage area A_{cr} in the headwaters of a channel (where log (S) and log (A) start to be correlated) and the top of the knickpoint k. The relict portion of the river was then projected

downstream. For the channels draining directly into the Drava River, which represent the regional base level and is well equilibrated (Robl et al., 2008), the relict segment was projected until the confluence with the Drava River and the Incision *I* refer the vertical difference between the extrapolated and present day profile at this particular point (Fig. 1.2). For the channels draining toward Miocene Basins, we have projected the channel profiles until the transition between crystalline basement and Basin because we cannot assume similar concavity and steepness indices for the two areas because of their different lithology. For these rivers the incision *I* refer to the vertical difference between projected and present day channel profile at the transition between crystalline basement and sedimentary basin.

1.3.3. Apatite (U-Th)/He-thermochronology

Apatite (U-Th)/He-thermochronology is useful to reconstruct the thermal history of the upper crust and use this as a proxy for morphological evolutions of the Earth´s surface (e.g. Ehlers and Farley, 2003). The closure temperature of AHe is often considered to be 70°C (Ehlers and Farley, 2003). More precisely the method is sensitive in the temperature range between approximately 80 ºC and 40 ºC (Wolf et al., 1998) which is called the Partial Retention Zone (PRZ). Depending on the geothermal gradient (typically between 25 °C/km and 40 °C/km), AHe thermochronology can record exhumation of rocks from about 1-4 km depth. The Ages reported are mean of AHe ages as single grain aliquots and at least one duplicate of every sample was measured. The AHe age for one sample is the mean of the different grains ages with a 1sigma error. Six replicate analyses of Durango apatite yielded a mean AHe age of 32.6 ± 1.5, which is in good agreement with the Durango apatite reference age of 31.44 ± 0.18 Ma (McDowell et al., 2005). Sample processing and He measurements were done in Tübingen. U, Th and Sm concentrations have been measured at University of Arizona.

1.4. Results

Using the methods discussed above, we have mapped incised relict landscapes in the two selected key regions. For the Pohorje Massif, our results are summarized in Fig. 1.3a,b. The black line separating the relict from the incised landscape on Fig. 1.3 and was mapped following the boundary of the low slope area (Fig. 1.3a) compared to the steeper incised

landscape. The highest elevation of the mapped relict landscape is the summit of the Pohorje Mountain (1543 m) and the lowest elevation is about 300 m in the southern part of the range, at the boundary with the Pannonian basin. No relationship can be seen between the extent of the incised and relict landscape with the boundary of the granite pluton (Fig. 1.2d). We conclude that the incised relict landscape of Pohorje is not related to lithology. The k_{sn} map (Fig. 1.3a) shows similar situation as the hillslopes with low k_{sn} values on the relict landscape and higher values for the incised landscape. Our mapping results for the Koralpe region are shown in Fig. 1.3c,d. The mapped relict landscape includes most of the Koralpe topography and its summit, the Speikkogel (2140 m). The lowest elevation of the mapped relict landscape is about 350 m at the eastern boundary of Koralpe. Much of the range is considered to be part of the relict landscape and only small areas in the catchments of the rivers, and their steep gorges are part of the newly incised landscape. We find that the relief map and the k_{sn} map (Fig. 1.3) match very well and show a well preserved incised relict landscape. Similar with Pohorje, we do not see any relationship between the relict landscape contour and the lithology (Fig. 1.2e). The slope distribution of the mapped relict landscapes display similar pattern for Koralpe and Pohorje (Fig. 1.3e) with an average slope of 13° and 12° , respectively. Both Koralpe and Pohorje relict landscape slope distributions are skewed toward low values (0.3) which indicate a predominance of low slopes over steep slopes. Koralpe and Pohorje incised landscape average 21° and 19° respectively with a slight skewness toward high slopes (-0.2). The slope distribution shows that both area display very similar morphometric patterns despite their different lithologies and exhumation history. The asymmetry of the Koralpe Mountain is well visible on Fig. 1.4, with a steep western slope, facing the Lavanttal Basin, and a gentle eastern slope facing the Styrian basin. Photographs of the mapped incised relict landscapes for the Pohorje and Koralpe regions are shown in Fig. 1.5.

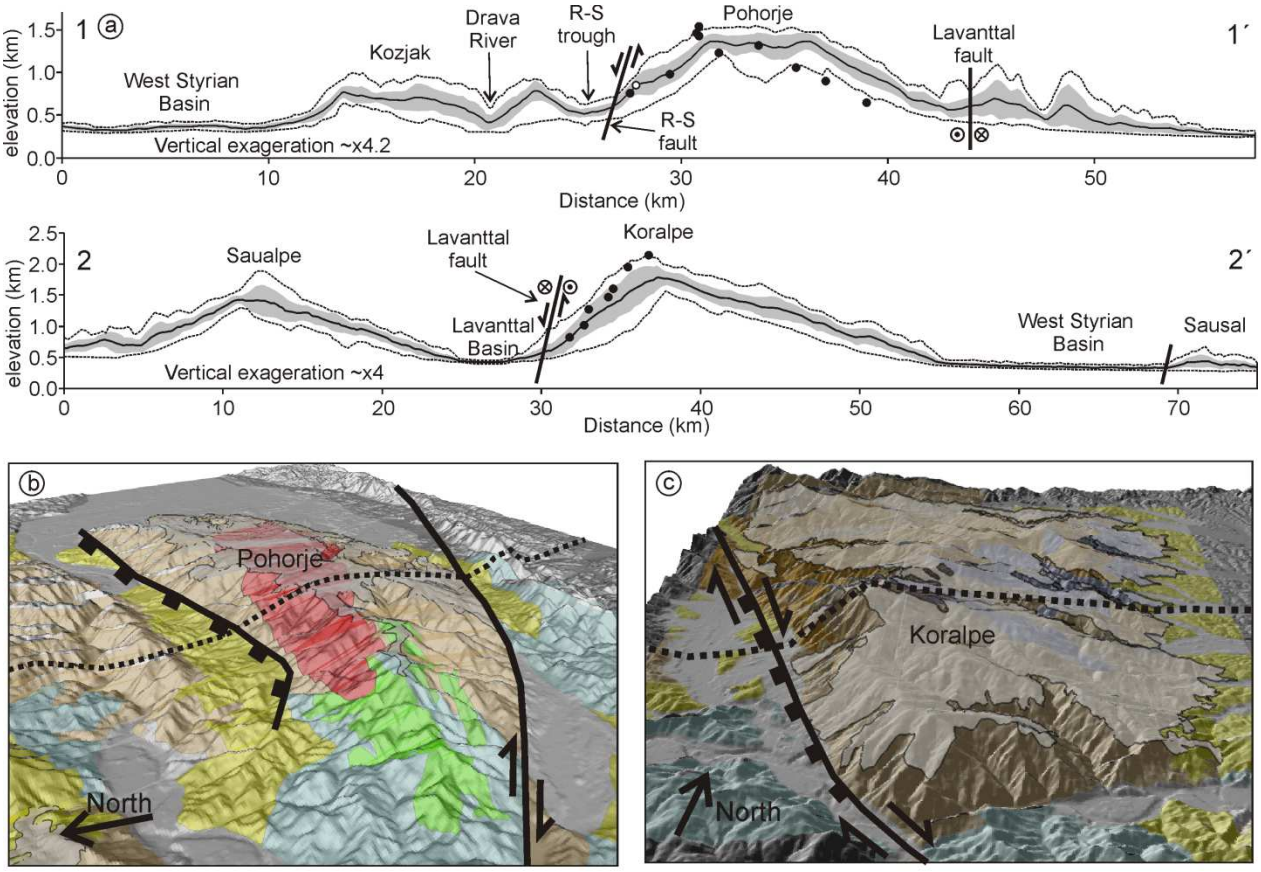

Figure 1.4: Swath profiles and oblique views of the Koralpe and Pohorje Mountains. (a) Swath profiles of Pohorje (1-1´) and Koralpe (2-2´); for location of the swaths see Fig. 1.1; Solid black line is mean elevation, grey area is the standard deviation and dashed lines are minimum and maximum elevations. Black and white Points represents the location of samples for apatite (U-Th)/He thermochronology, or their projection when they are located outside of the swath. On the Pohorje profile, the white point refers to the sample P2 which is a volcanic dyke; all other samples are from the granite; R-S: Ribnica-Selnica. (c) Oblique view of Pohorje from the North West. Grey transparent polygon is the mapped relict landscape. Lithology: yellow: Miocene sediments; blue: Pre-Miocene sedimentary rocks; green: volcanic rocks (Dacite); light brown: Austroalpine gneiss. The crosscutting relationship between the Granite and the relict landscape is well visible. Dashed line represents approximately the trace of the swath profile. (d) Oblique view of Koralpe from the South. Grey transparent polygon is the mapped relict landscape. Lithology: same as for Pohorje and: orange: micaschist; purple on the eastern slope of Koralpe: Mylonitic gneiss (Plattengneiss). Dashed line represents approximately the trace of the swath profile.

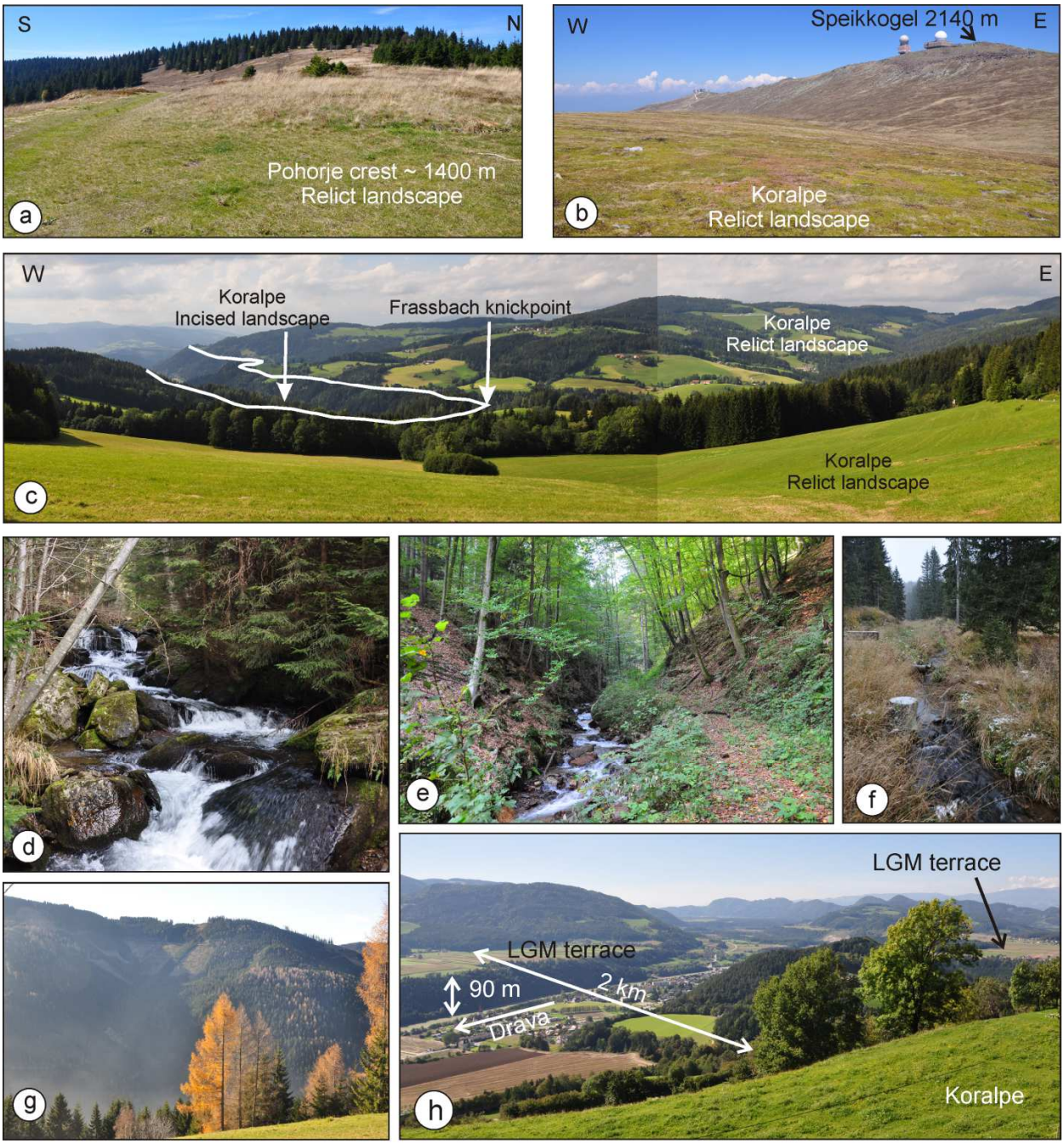

Figure 1.5: Photographs of the investigated regions and their incised relict landscapes. (a) View of the very smooth crest of Pohorje forming part of the relict landscape. (b) View from the southwest of the Koralpe summit (Speikkogel). This side of the Koralpe summit was not affected by LGM glacier carving and the small glacier cirques are located on the northeast side of the summit, behind the crest in the background. (c) View to the North of the Frassbach catchment and knickpoint (projected River number 3), white line is the break-in-slope between the relict and incised landscape. (d) View looking upstream of the Prössingbach river (located to the south of the Frassbach River) in the incised landscape, the channel features many small waterfalls and bedrock outcrops are visible. (e) Steep hillslopes in the Koralpe incised landscape. (f) View looking upstream of the Prössingbach River on the relict landscape (compare to Figure 1.5d), the river is flowing on its own deposits (alluvial) and no bedrock outcrop in the channel is present. (g) View to the South, from the crest between Prössingbach and Frassbach, into the Prössingbach incised valley showing the steep hillslopes of the incised landscape; (h) View to the North West from Koralpe of the Drava river LGM terraces in the last visible part of the Drava valley in the background is the terminal moraine from LGM.

1.4.1. Quantification of the amount of incision

In order to quantify the amount of incision into the Koralpe and Pohorje landscape we use the projection method described in section 1.3.2. Four of the eight selected channels drain the Koralpe Mountain towards the Miocene basins: the Waldensteinerbach, the Fallegbach and the Schwarze Sulm that drain into the Styrian basin in the East before to join the Mur river, and the Frassbach that drain to the Lavanttal basin to the West before to join the Drava river (Fig. 1.6). The other four selected channels drain directly into the Drava River (Fig. 1.7) and are: the Radoljna River and the Lobnica River from the Pohorje Mountain; the Krennbach River and the Feistritz River from Koralpe. The calculated amount of incision averages 387 ± 105 m for the eight investigated rivers (Table 1.1). The calculated amount of incision of the Pohorje rivers is slightly higher than the one from the Koralpe channels. However the calculated amount of incision from the two Pohorje channels is associated with higher uncertainty (Table 1.1). Considering their large uncertainty, the incision amounts of the Pohorje channels are not higher than the average incision amount of the Koralpe channel alone. Because they are undistinguishable considering the uncertainty on the calculated amount of incision of each river, we do not interpret the Koralpe and Pohorje amount of incision separately, for example to infer differential uplift between the two areas. Whether the incision is related to surface uplift of the Koralpe and Pohorje mountains or to simple incision will be discussed later (Section 1.5).

Table 1.1: Channel profiles analysis for the 8 selected rivers.

ID	Name	A_{min}[a] (m²)	A_{max}[a] (m²)	θ	±2σ	k_s	±2σ	k_{sn}[b]	±2σ	r²	I[c] (m)	±2σ
Relict												
1	Waldensteinerbach	3.40E+05	3.20E+07	0.55	0.05	2.28E+02	9.91E+00	46	2	0.71	241	22
2	Fallegbach	6.00E+05	5.80E+06	0.69	0.11	1.59E+03	1.30E+02	49	4	0.90	403	67
3	Frassbach	2.50E+05	2.60E+07	0.43	0.03	6.60E+01	1.39E+00	95	2	0.94	216	15
4	Schwarze Sulm	5.20E+06	1.80E+07	0.89	0.18	1.14E+05	6.13E+03	93	5	0.87	372	76
5	Krennbach	1.20E+06	6.30E+06	0.65	0.13	1.96E+03	6.76E+01	87	3	0.86	480	97
6	Feistritz	5.80E+05	2.40E+07	0.48	0.07	8.70E+01	3.16E+00	55	2	0.91	380	56
7	Rodoljna	3.00E+05	5.10E+06	0.26	0.09	2.21E+00	2.85E-01	31	4	0.89	477	173
8	Lobnica	2.20E+04	3.40E+06	0.39	0.17	8.25E+00	1.18E+00	14	2	0.80	527	240
											387	**105**
Knickzone												
1	Waldensteinerbach	-	-	-	-	-	-	-	-	-		
2	Fallegbach	6.30E+06	1.10E+07	3.50	0.49	1.03E+23	5.72E+21	162	9	0.84		
3	Frassbach	2.90E+07	3.60E+07	3.90	0.75	4.29E+33	3.02E+32	270	19	0.85		
4	Schwarze Sulm	2.00E+07	6.70E+07	0.86	0.17	2.00E+05	2.88E+03	139	2	0.68		
5	Krennbach	-	-	-	-	-	-	-	-	-		
6	Feistritz	3.40E+07	7.20E+07	2.20	0.39	6.75E+15	2.87E+14	188	8	0.77		
7	Rodoljna	9.50E+06	6.30E+07	0.88	0.12	2.01E+05	6.88E+03	146	5	0.82		
8	Lobnica	1.90E+07	6.00E+07	1.80	0.23	6.18E+12	2.93E+11	169	8	0.85		

All fitted channels were smoothed with a 500 m moving window and a vertical sampling interval of 15 m was used.

[a] A_{min} is the minimum drainage area used for the fit and A_{max} is the maximum drainage area used for the fit

[b] k_{sn} was calculated with a reference concavity index of 0.45.

[c] I refer to the calculated incision in m; bold number is mean incision amount for all channels, with standard deviation around the mean.

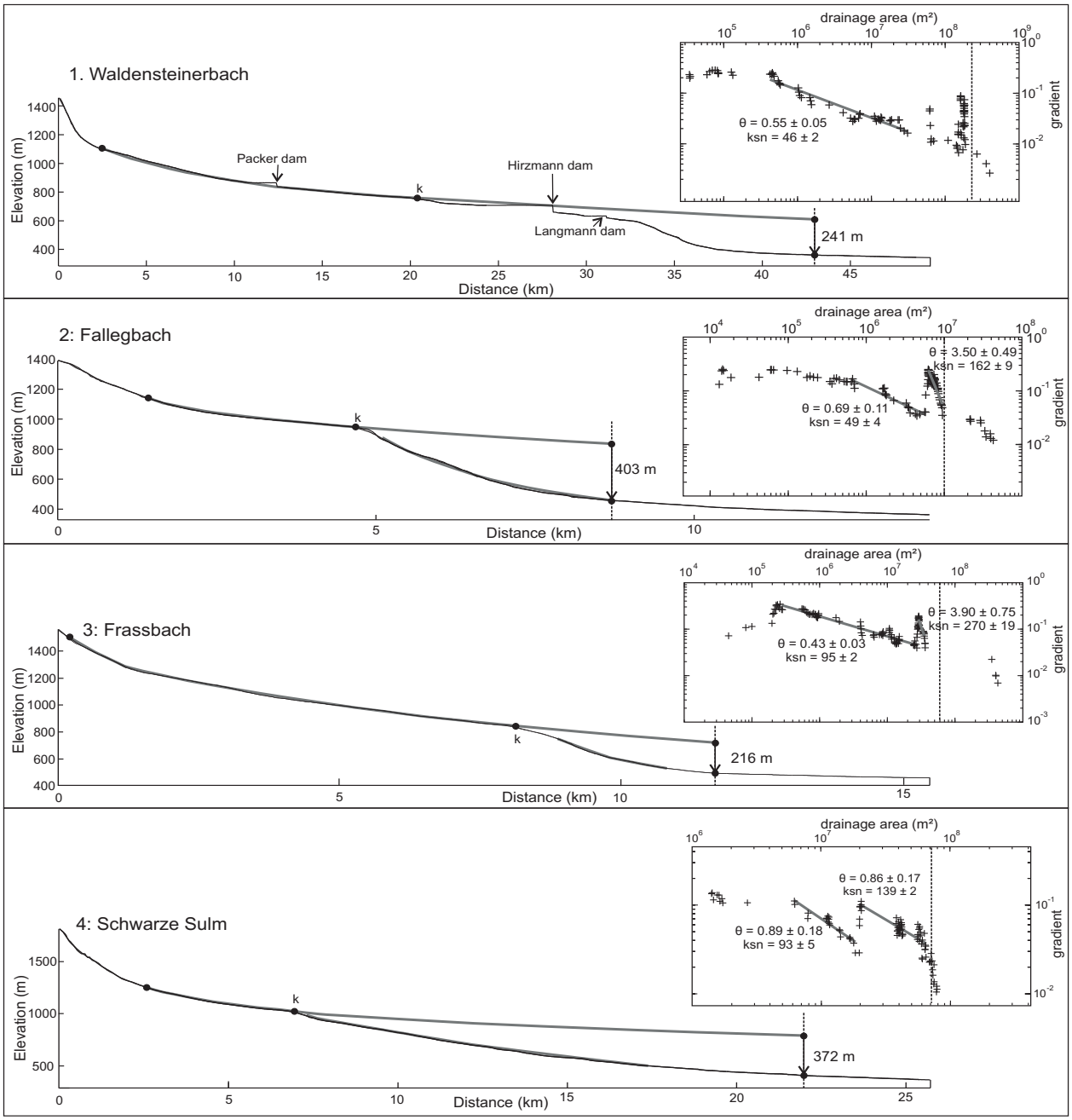

Figure 6
Legrain et al., 2013

Figure 1.6: Channel profile projection for the 4 selected channels of Koralpe draining to Miocene Basins. For location of the channels refer to Figure 1.3. Thin black lines are the raw and the smoothed channel profiles, thick grey lines are the fitted segments; *k*: knickpoint. The vertical dashed lines in the different plots are the location of the transition between crystalline basement and basin where the incision amount is calculated. For detailed method and parameters used for the slope-area plots refer to Table 1.1.

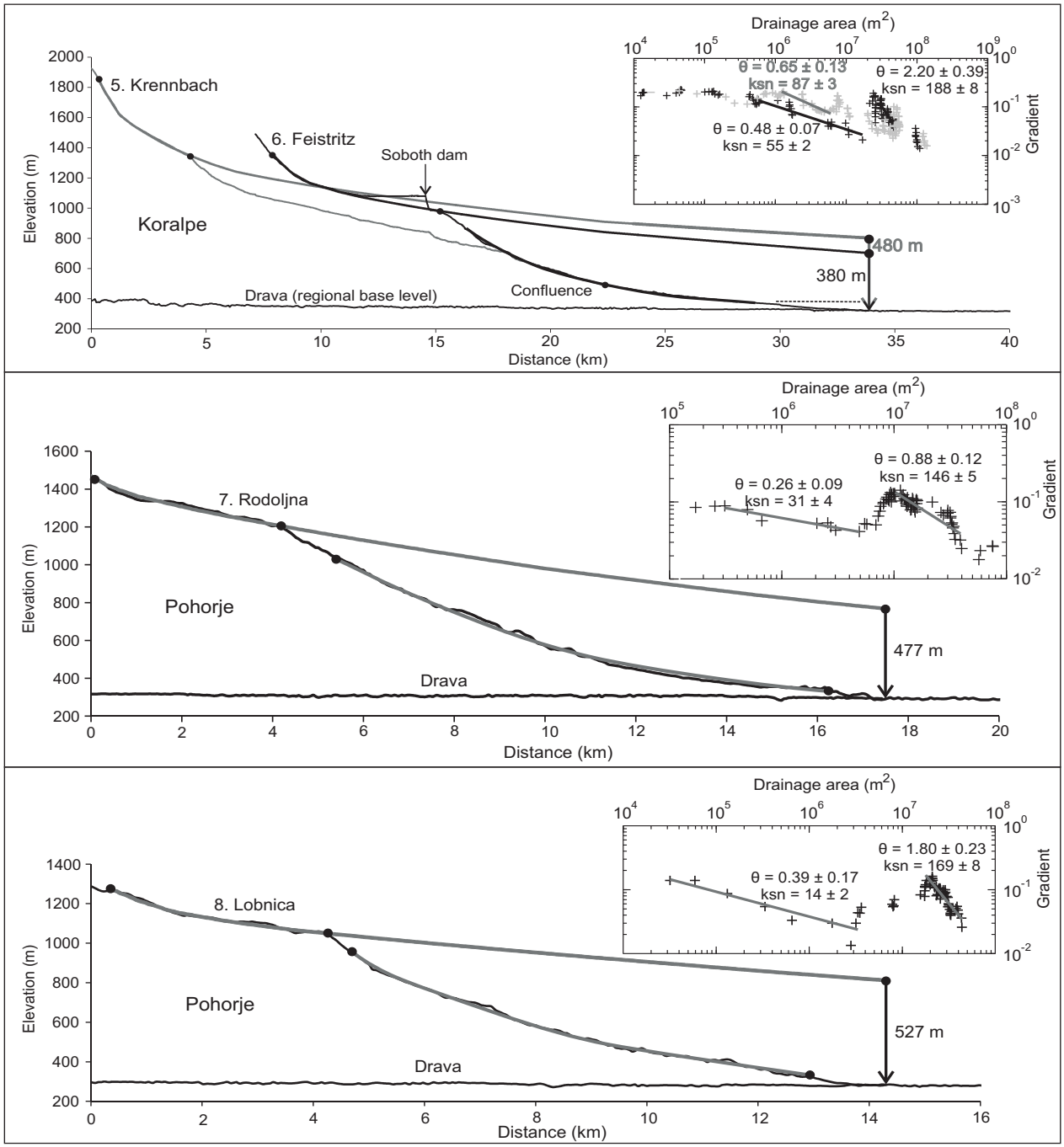

Figure 7
Legrain et al., 2013

Figure 1.7: Channel profile projection for the 4 selected channels of Koralpe and Pohorje draining to the Drava River. For location of the channels refer to Fig. 1.3. Thin black lines are the raw and the smoothed channel profiles, thick grey lines are the fitted segments; *k*: knickpoint; horizontal dashed line on the Koralpe rivers plot is the top of a fill fluvial terrace of the Drava river from the LGM. For detailed method and parameters used for the slope-area plots refer to Table 1.1

1.4.2. Time constraints on the formation of the relict landscapes

The results of the channels projection have shown that only several hundreds of meters (~ 400 m) have been incised in the two studied regions, which is not enough to be recorded by AHe ages (see section 1.3.3). However, the AHe ages can provide time constraints on the formation of the relict landscapes prior to the incision and, very important, the link between the relict landscapes and the active faulting that took place during the Early Miocene, in the frame of the lateral extrusion of the Eastern Alps. More precisely, we aim to determine if: (1) The relict landscapes have formed before the Early Miocene active faulting and represent deformed pre-Miocene landscapes that can be used as a deformation and uplift passive markers; (2) They have formed after the Early Miocene and cannot be considered as Pre-Miocene deformed surfaces.

In order to solve this question we have collected in total 20 samples from Koralpe and Pohorje (Table 1.2 and 1.3). From Koralpe, 9 samples were analyzed and the AHe ages range between 21.4 ± 6.2 Ma and 34.3 ± 1.5 Ma (Table 1.2, 1.3, Fig. 1.8) The western slope of Koralpe is directly facing the Lavanttal fault (Fig. 1.4, 1.8) and the samples KOR 1 to KOR 7 were taken to form an age-elevation profile from the Koralpe summit at 2140 m elevation down toward the Lavanttal valley at 1015 m elevation (Fig. 1.4b, 1.8). In addition, two more samples (one from high elevation, and one from low elevation) where taken from atransect further south plus one sample from further north intheKoralpe region.

Table 1.2: Analytical results for AHe ages with calculated single grains and mean ages.

Sample	4-He (mol)	238-U (mol)	235-U (mol)	232-Th (mol)	147-Sm (mol)	Uncorr. Age (Ma)	Ft	Alpha-corr. Age (Ma)	Mean Age (Ma)	±1σ
				Pohorje						
PO2 #1	1.75E-14	9.57E-13	7.08E-15	1.18E-13	5.72E-13	13.7	0.78	17.5	18.9	1.9
#2	8.98E-15	4.18E-13	3.09E-15	1.22E-13	2.78E-13	15.5	0.77	20.2		
PO3 #1	6.10E-15	3.76E-13	2.78E-15	6.09E-14	6.22E-14	12.1	0.71	17.1	17.5	0.6
#2	5.14E-15	2.28E-13	1.69E-15	3.08E-13	2.77E-13	13.3	0.74	18.0		
PO4 #1	3.92E-15	2.12E-13	1.57E-15	1.82E-13	3.11E-13	11.9	0.77	15.3	18.6	3.5
#2	2.67E-15	1.42E-13	1.05E-15	1.01E-13	1.34E-13	12.5	0.69	18.2		
#3	1.04E-14	4.54E-13	3.36E-15	1.66E-13	2.39E-13	16.4	0.73	22.3		
PO5 #1	7.93E-15	3.44E-13	2.55E-15	3.86E-13	5.10E-13	14.1	0.79	17.9	20.4	2.5
#2	6.94E-15	2.69E-13	1.99E-15	2.12E-13	3.12E-13	16.8	0.74	22.9		
#3	1.27E-14	5.57E-13	4.12E-15	2.53E-13	1.08E-12	15.9	0.78	20.5		

PO6 #1	8.79E-15	4.38E-13	3.24E-15	2.33E-13	2.28E-13	13.8	0.76	18.3	16.7	1.4
#2	2.75E-15	1.54E-13	1.14E-15	6.71E-14	2.25E-13	12.5	0.78	16.1		
#3	9.35E-15	4.93E-13	3.65E-15	3.27E-13	6.35E-13	12.7	0.81	15.7		
PO7 #1	2.95E-15	1.62E-13	1.20E-15	1.68E-13	3.19E-13	11.3	0.72	15.7	16.7	1.4
#2	5.53E-15	2.35E-13	1.74E-15	3.74E-13	4.08E-13	13.3	0.75	17.7		
P1 #1	3.06E-15	1.23E-13	9.07E-16	2.24E-13	2.93E-13	13.5	0.71	19.1	17.8	2.2
#2	2.94E-15	1.60E-13	1.18E-15	2.04E-13	2.86E-13	10.9	0.72	15.3		
#3	1.36E-15	6.52E-14	4.82E-16	6.97E-14	1.27E-13	12.8	0.67	19.1		
P2 #1	3.98E-15	2.49E-13	1.84E-15	1.04E-13	4.30E-13	11.2	0.68	16.4	13.9	2.3
#2	2.43E-15	1.84E-13	1.36E-15	1.29E-13	2.24E-13	8.8	0.74	11.8		
#3	8.26E-15	5.54E-13	4.10E-15	1.17E-13	1.39E-13	11.0	0.81	13.6		
P3 #1	5.95E-15	3.50E-13	2.59E-15	1.57E-13	4.19E-13	11.9	0.77	15.4	16.4	1.2
#2	4.26E-14	2.04E-12	1.51E-14	6.50E-13	1.59E-12	15.0	0.85	17.7		
#3	6.11E-15	3.31E-13	2.45E-15	2.06E-13	3.81E-13	12.4	0.78	16.0		
P5 #1	9.31E-15	4.71E-13	3.48E-15	2.41E-13	5.91E-13	13.6	0.76	18.0	16.7	1.1
#2	2.55E-14	1.35E-12	1.00E-14	8.19E-13	1.82E-12	12.8	0.80	16.0		
#3	6.20E-15	3.56E-13	2.64E-15	1.74E-13	4.41E-13	12.0	0.75	16.1		
P6 #1	8.93E-15	4.59E-13	3.39E-15	2.62E-13	4.75E-13	13.3	0.77	17.3	17.8	0.8
#2	3.77E-15	1.82E-13	1.34E-15	1.59E-13	2.52E-13	13.3	0.73	18.3		

Koralpe

K1 #1	1.12E-14	3.16E-13	2.34E-15	4.33E-14	1.83E-12	25.9	0.78	33.1	33.4	0.6
#2	2.47E-14	6.69E-13	4.95E-15	9.36E-14	1.80E-12	27.3	0.83	33.0		
#3	1.16E-14	3.23E-13	2.39E-15	3.59E-14	1.55E-12	26.4	0.77	34.1		
K3 #1	2.74E-15	8.49E-14	6.28E-16	4.17E-14	1.20E-13	22.3	0.79	28.1	21.4	6.2
#2	1.76E-15	9.96E-14	7.37E-16	1.38E-14	1.54E-13	13.1	0.82	16.0		
#3	1.34E-15	6.54E-14	4.84E-16	1.57E-14	9.76E-14	14.9	0.74	20.2		
K5 #1	1.08E-14	3.01E-13	2.23E-15	2.48E-14	1.02E-13	27.0	0.81	33.2	34.3	1.5
#2	3.48E-15	8.60E-14	6.36E-16	2.04E-14	2.15E-13	29.3	0.83	35.4		
KOR1 #1	6.65E-14	1.93E-12	1.43E-14	1.78E-13	2.64E-13	26.0	0.86	30.2	31.3	3.0
#2	1.19E-14	3.14E-13	2.32E-15	1.60E-14	1.49E-13	28.8	0.83	34.7		
#3	2.33E-14	7.37E-13	5.45E-15	5.84E-14	8.40E-14	24.0	0.82	29.1		
KOR2 #1	1.04E-14	3.65E-13	2.70E-15	5.25E-14	6.56E-13	21.1	0.78	26.9	25.6	1.4
#2	8.30E-15	3.26E-13	2.41E-15	6.97E-14	5.17E-13	18.6	0.77	24.2		
#3	1.78E-14	6.30E-13	4.66E-15	8.38E-14	1.13E-12	20.9	0.81	25.8		
KOR4 #1	2.45E-15	9.86E-14	7.30E-16	5.69E-15	2.74E-14	18.9	0.81	23.4	24.2	1.7
#2	5.11E-15	1.87E-13	1.38E-15	1.86E-14	2.94E-14	20.6	0.79	26.1		
#3	3.36E-15	1.35E-13	1.00E-15	8.47E-15	3.17E-14	18.9	0.82	23.1		
KOR5 #1	1.26E-14	4.48E-13	3.31E-15	1.91E-14	4.30E-13	21.5	0.80	26.9	23.4	4.9
#2	4.29E-15	2.04E-13	1.51E-15	4.51E-14	1.11E-13	15.5	0.77	20.0		
KOR6 #1	5.88E-15	1.80E-13	1.33E-15	3.11E-14	5.20E-13	24.0	0.77	30.9	25.6	4.3
#2	6.18E-15	2.45E-13	1.81E-15	2.32E-14	5.61E-13	18.9	0.78	24.3		
#3	6.24E-15	2.26E-13	1.67E-15	2.67E-14	6.41E-13	20.5	0.77	26.5		
#4	4.76E-16	2.03E-14	1.50E-16	7.25E-15	5.23E-14	16.6	0.80	20.7		
KOR7 #1	5.01E-15	2.16E-13	1.60E-15	8.28E-14	4.08E-13	16.3	0.76	21.4	23.7	1.9
#2	5.85E-15	2.39E-13	1.77E-15	5.87E-14	4.73E-13	17.7	0.76	23.3		

#3	4.12E-14	1.25E-12	9.26E-15	8.74E-13	1.84E-12	21.8	0.84	26.0
#4	5.76E-15	2.22E-13	1.64E-15	7.57E-14	3.94E-13	18.5	0.76	24.3
Blank #1	4.66E-17	2.22E-16	1.64E-18	5.54E-17	-6.96E-15			
#2	4.66E-17	2.22E-16	1.64E-18	5.54E-17	-6.96E-15			
Dur. #1	5.53E-14	2.56E-13	1.89E-15	4.51E-12	8.69E-13	33.3		
#2	1.30E-13	5.45E-13	4.03E-15	1.07E-11	2.20E-12	33.8		
#3	1.14E-13	4.97E-13	3.68E-15	9.40E-12	2.33E-12	33.4		
#4	2.23E-13	1.02E-12	7.54E-15	1.83E-11	3.70E-12	33.1		
#5	1.08E-13	5.35E-13	3.96E-15	1.01E-11	1.83E-12	29.3		
#6	1.88E-13	8.17E-13	6.04E-15	1.58E-11	3.41E-12	32.9		

For location and elevation of the samples refer to Table 1.3. Dur. refers to Durango apatite measurements that were performed during this work (6 replicates).

Table 1.3: Results of AHe ages measured in this study with geographic coordinates and elevation of the samples.

Sample	Longitude[a]	Latitude[a]	Elevation (m)	AHe age (Ma)	± 1σ
		Pohorje			
PO2	15.432	46.423	637	18.9	1.9
PO3	15.390	46.442	887	17.5	0.6
PO4	15.373	46.454	1042	18.6	3.5
PO 5	15.335	46.471	1297	20.4	2.5
PO6	15.333	46.489	1211	16.7	1.4
PO7	15.340	46.510	966	16.7	1.4
P1	15.268	46.528	746	17.8	2.2
P2	15.269	46.525	840	13.9	2.3
P3	15.260	46.498	1409	16.4	1.2
P5	15.255	46.497	1517	16.7	1.1
P6	15.264	46.498	1437	17.8	0.8
		Koralpe			
K1	15.017	46.987	791	33.4	0.6
K3	14.976	46.631	823	21.4	6.2
K5	15.035	46.684	1076	30.0	7.5
KOR1	14.972	46.787	2140	31.3	3.0
KOR2	14.955	46.791	1949	25.6	1.4
KOR4	14.943	46.786	1603	24.2	1.7
KOR5	14.938	46.782	1467	23.4	4.9
KOR6	14.922	46.784	1273	25.6	4.3
KOR7	14.919	46.771	1015	23.7	1.9

[a] Coordinates are in decimal degrees (WGS84)

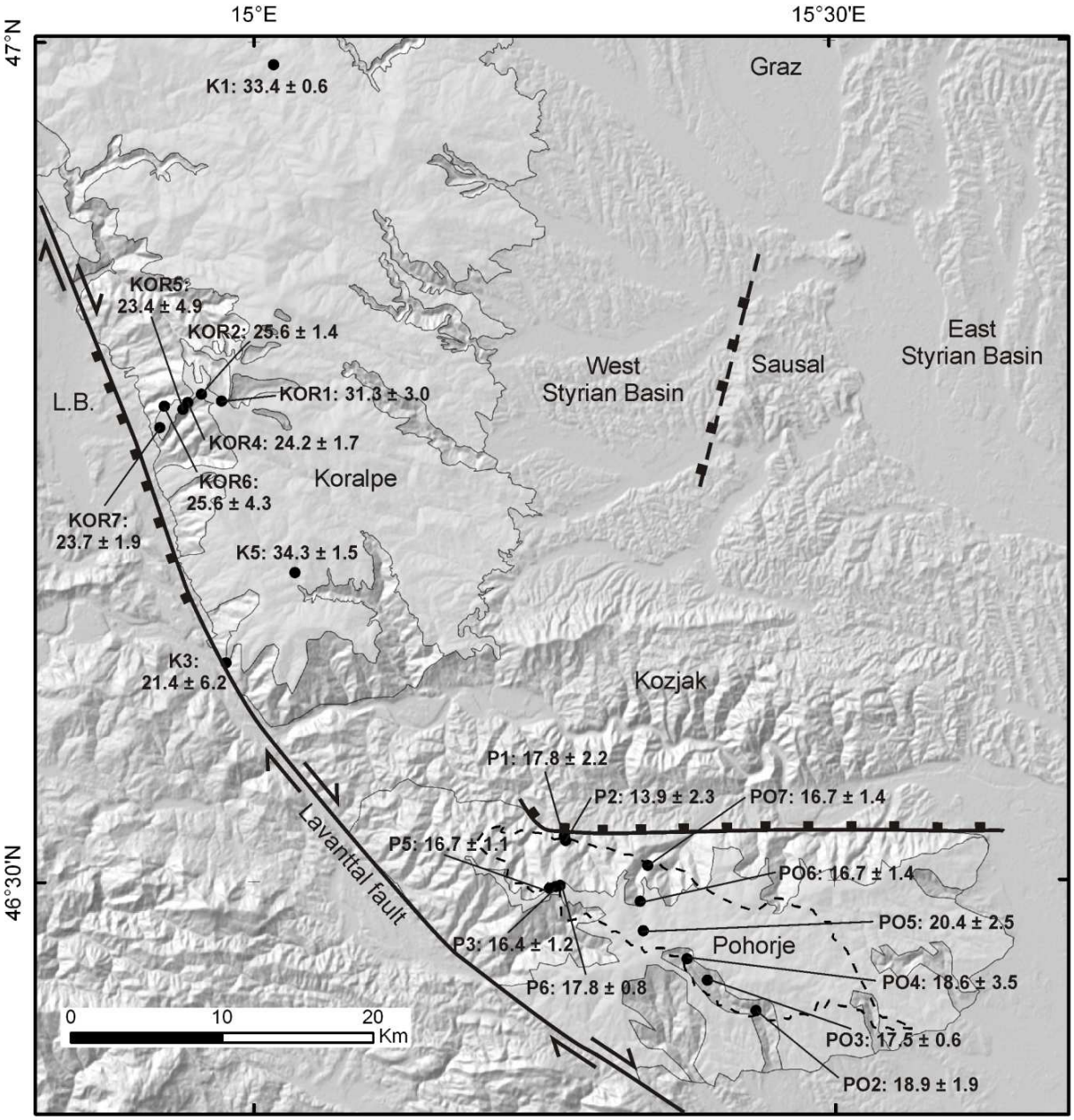

Figure 1.8: Results of apatite (U-Th)/He thermochronology. Ages are AHe ages in Ma ± 1σ; white polygons are the mapped relict landscapes; dashed black line is the boundary of the Pohorje granite.

The samples from the western slope show a moderate linear fit (r^2 = 0.54) with an inferred exhumation rate of 105 m/Ma from 31 to 21 Ma (Fig. 1.9a). This exhumation rate is very similar to the one documented from apatite fission track data obtained by Hejl (1997) (82 m/Ma) indicating a steady exhumation history of about 100 m/Ma from the Eocene into the early Miocene and possibly to the present. This indicates that the Koralpe has experienced very little exhumation during the whole Miocene and the Koralpe AHe ages were apparently not affected by the tectonically very active Early Miocene period (18 Ma to 16 Ma).

We have measured 10 AHe ages from the Pohorje Mountain. Nine samples were taken from the granite, and one from a volcanic dyke of dacite (Fig. 1.8, sample P2). The AHe ages from the granite range between 20.4 ± 2.5 Ma and 18.9 ± 1.9 Ma while the measured AHe age from the volcanic dyke is younger: 13.9 ± 2.3 Ma. The AHe ages are not correlated with elevation and are in the same range of ages regardless of the elevation of the samples (Fig. 1.9). The measured AHe ages from the granitic samples are very homogeneous and suggest that all samples had cooled down below 70° C by ~15 Ma. The Pohorje pluton probably intruded the Austroalpine unit at a very shallow level where ambient temperatures were below 70 °C. However, the apparent very fast exhumation of the granite cannot be only related to cooling due to crystallization of the magma into granite because granitic pebbles have been found in 17 Ma old sediments in the adjacent sedimentary basins (Fodor et al., 2008). So at least a part of this fast cooling is related to real exhumation (i.e. movement toward the surface) because some parts of the pluton were already at the surface by 17 Ma (Fig. 1.9). As already interpreted by Sachsenhofer et al. (1998), and considering the tectonic context of the Pohorje Mountain (Fig. 1.3), this very fast exhumation is probably more due to tectonic denudation from normal faulting of the Ribnica Fault, rather than to simple erosion. Regardless of the relative proportion of erosion and tectonic denudation, and considering that the relict landscape of Pohorje is developed onto and cross cut the granite, we can infer that the relict landscape is younger than the granite. Indeed, the relict landscape cannot be older than the intrusion of the granite and its exhumation to the surface, because our ages support the idea of a very fast process that is incompatible with the preservation of any older landform. Thus, our AHe ages from Pohorje give an upper bound for the creation of the Pohorje relict landscape that cannot be older than 15 Ma, the youngest measured AHe age when taking in account the error bars (Fig. 1.8b).

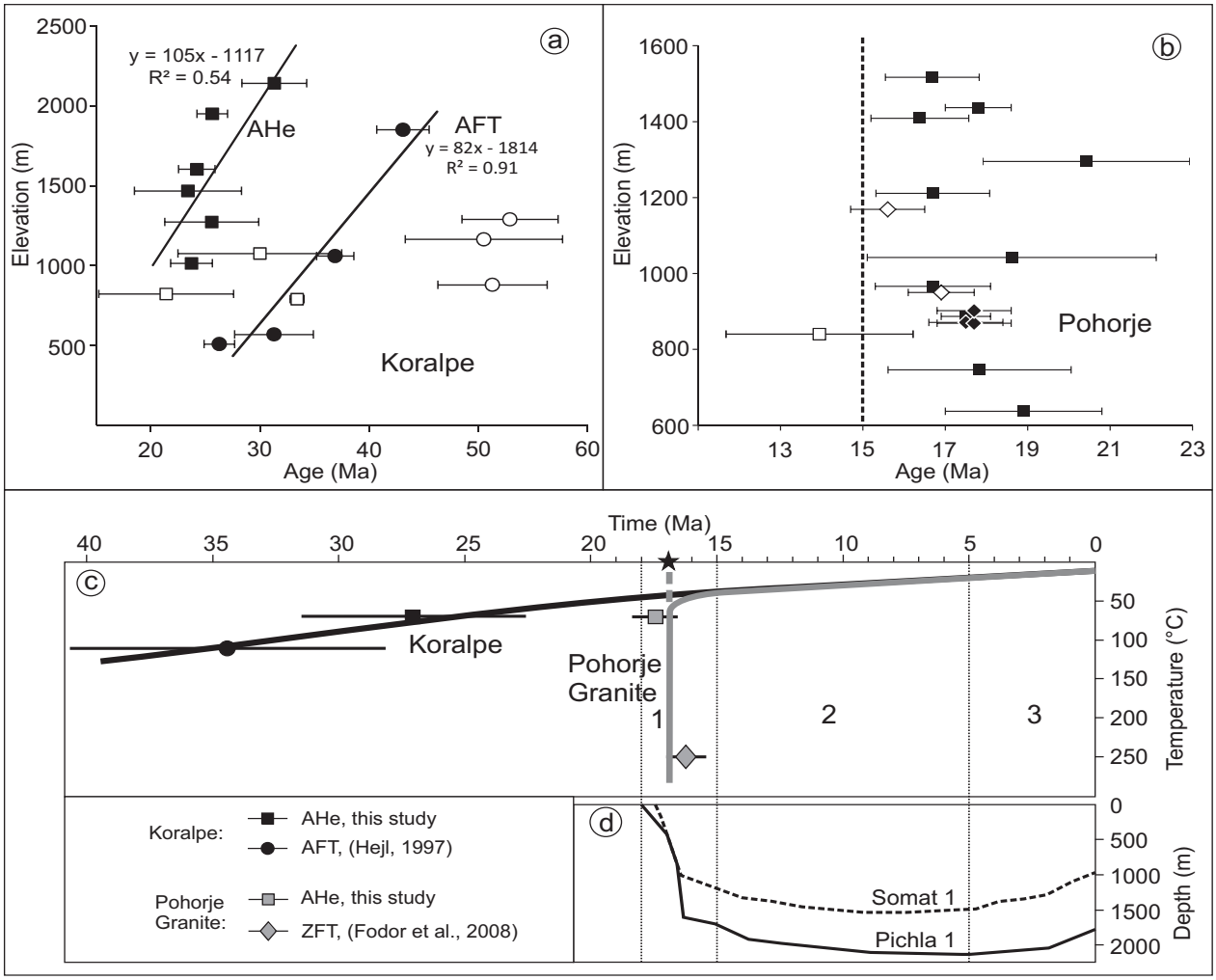

Figure 9
Legrain et al., 2013

Figure 1.9: Age-elevation relationship of thermochronology data and cooling paths of the Koralpe and Pohorje mountains. (a) Age-elevation relationship of Koralpe. Squares are AHe ages (this study); black squares are the samples of the profile taken from the western slope of Koralpe (samples Kor 1 to Kor 7) that are included for the linear regression (black line); white squares are the samples located in other parts of Koralpe. Circles are AFT ages (Hejl, 1997); Black circles are included in the linear regression and white circles are from other locations in Koralpe (see Hejl, 1997 for location of the samples and details of the linear regression). (b) Age-elevation relationship of Pohorje. Squares are AHe ages (this study); black squares are granitic samples and the white square is the volcanic rock sample (P2); Diamonds are ZFT ages (Fodor et al., 2008); Black diamonds are granitic samples and white diamonds are volcanic rock samples (dacite). See Fodor et al. (2008) for location of the ZFT samples. Vertical dashed line represents the youngest AHe age from the granitic samples considering error bars (15 Ma). (c) Cooling path for Koralpe and Pohorje based on the different thermochronological ages. Symbols are mean ages for the entire area with error bars representing the standard deviation around the mean. Thick lines are inferred cooling paths for Koralpe and Pohorje. The black star refers to the oldest known sediments where magmatic pebbles have been found (Fodor et al. 2008); thick dashed grey line indicate exhumation of part of Pohorje granite to the surface. Vertical lines and numbers refer to the different period discussed in the text for the interpretation of the tectonic and landscape evolution of the area. (d) Subsidence curves of two wells (Somat 1, Pichla 1) of the Styrian basins (Ebner and Sachsenhofer, 1995; Sachsenhofer et al., 1998; 2001); see Fig.1.1 for location of the wells.

1.5. Discussion

In the following section we infer an integrated landscape evolution scenario of the studied area, the south eastern corner of the Alps, since the Early Miocene. The inferred scenario is based on different datasets that include: (1) our morphometric analysis and our new AHe ages, (2) existing low-temperature thermochronological ages, (3) existing subsidence analysis of the Miocene basins. This inferred scenario for the Early to late Miocene evolution of the area is summarized in Fig. 1.10. As discussed above, our AHe ages show that, by 15 Ma, the Pohorje pluton was not yet exhumed and can be used as an upper bound for the creation of the relict landscape. For the Koralpe landscape, AHe ages cannot directly give constraints on the relict landscape formation timing. The Koralpe Mountain has been considered as an eastward tilted block (Neubauer and Genser, 1990) and the asymmetry of the Koralpe Mountain is nicely visible on Fig. 1.3. In this context, if the relict would be older than the tilting, the relict landscape should only be present on the eastern slope of Koralpe and would have been disrupted by the Lavanttal Fault. However, the morphometric analysis has revealed that the Koralpe relict landscape is not only developed on the eastern gentle slope but on both sides of the range (Fig. 1.3, 1.4). This result suggests that the creation of the Koralpe relict landscape postdates the tilting. The tilting itself has not been directly dated, but by analogy with the rapid subsidence of the Lavanttal and West Styrian basins between 18 and 16 Ma, the tilting of Koralpe likely occurred during this period (Neubauer and Genser, 1990). This indirect time constraint on the creation of the Koralpe relict landscape suggests that the Koralpe relict landscape was created after ~16 Ma.

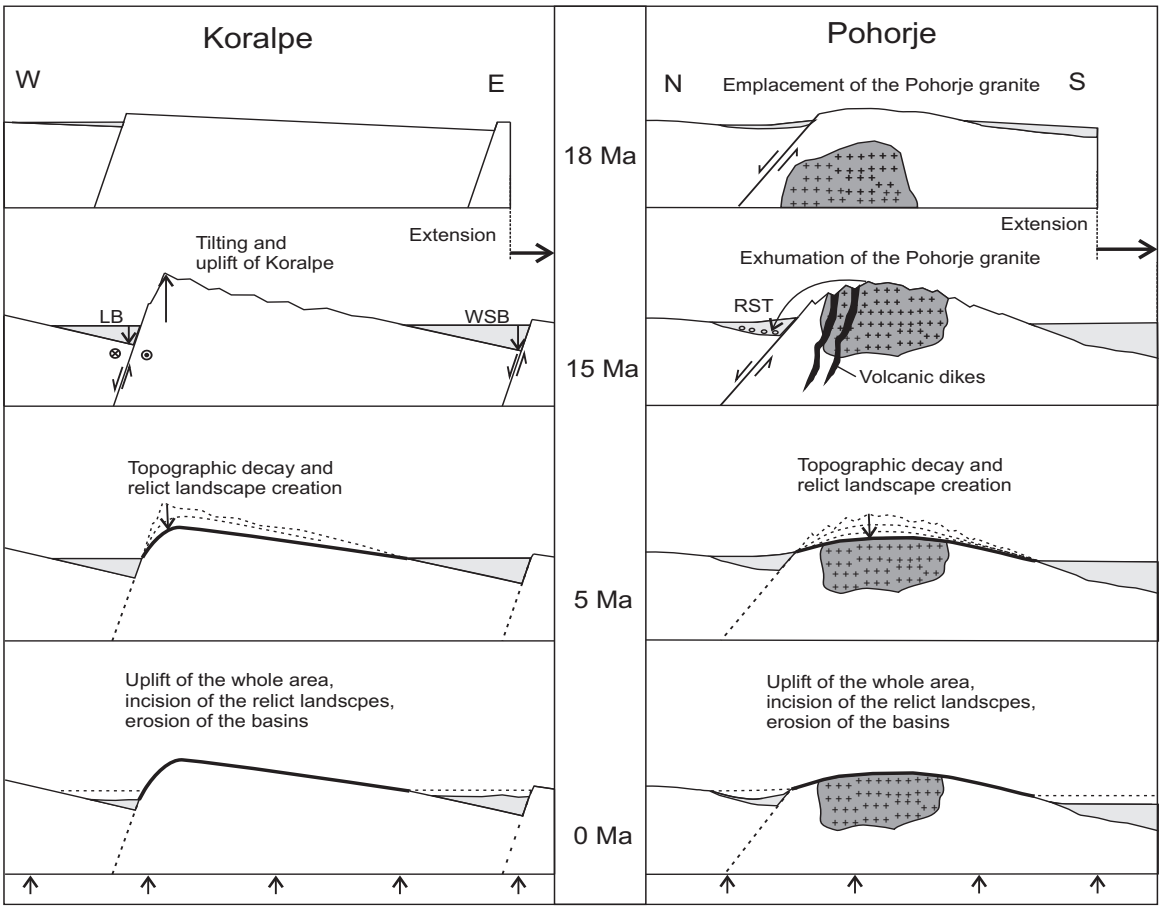

Figure 10
Legrain et al., 2013

Figure 1.10: Inferred scenario for the landscape and tectonic evolution of the studied area since the Early Miocene. Schematic cross-section of Koralpe and Pohorje (not to scale) with different time steps depicting tectonic processes and landscape evolution.

Taken together, both the Pohorje and Koralpe relict landscape seem to postdate the very active 18 Ma to 16-15 Ma period, during the main activity of the lateral extrusion of the Eastern Alps. As a consequence, the Koralpe and Pohorje relict landscape probably do not represent pre-Miocene dissected and deformed relict landscapes. While it seems clear that the relict landscapes are younger than 16-15 Ma, the exact timing of their creation and incision cannot be resolved only by our results. Subsidence analysis of adjacent basins can give us some constraints, even though indirect, on the landscape and uplift evolution of Koralpe and Pohorje for the missing time span (15 Ma to the present). We have selected subsidence curves from two wells (Fig. 1.9d, Ebner and Sachsenhofer, 1995; Sachsenhofer et al., 1998; 2001) that have recorded vertical movements for the last 18 Ma and are located in the vicinity of Koralpe and Pohorje, in the southern part of the Eastern Styrian Basin (see Fig. 1.1 for location of the wells). These subsidence curves as well as other datasets have been interpreted in details and we do not want to discuss here the detailed sedimentological and tectonic

interpretations (Ebner and Sachsenhofer, 1995; Sachsenhofer et al., 1998; 2001). Instead, in the following, we describe in a simple way these curves and compare them with our analysis of relict landscape to infer how these different observations can be integrated in a consistent scenario.

The two subsidence curves indicate that this part of the Styrian Basin started to subside very fast between 18 Ma and 16 Ma (Fig. 1.9d). From 16 to 12 Ma, a slower subsidence rate followed by a steady situation (from 12 to 5 Ma) occurred. Around 6-5 Ma, the basins started to be uplifted and this situation prevailed until the present. The estimated amount of uplift since the inversion of the basins from subsidence analysis of these two wells is 400-600 m (Ebner and Sachsenhofer, 1995; Sachsenhofer et al., 1998; 2001) and matches relatively well with the amount of incision that we have calculated from channel profile projection of the channels (387 ± 105 m). This inversion of the basins and associated increased rock uplift rate in the whole area, including the mountain ranges surrounding the basins, could explain very well the incision into the relict landscape. Thus, even though we could not directly date the incision into the relict landscapes, it is tempting to suggest that the described incision and the uplift of the basin are the result of the same mechanism. Another interesting comparison is possible with the incision of the Mur River North of Graz, which incised at a rate of approximately 100 m/Ma for the last 4 Ma, as inferred from cave sediments burial age dating (Wagner et al., 2010). If the uplift and incision did start around 5 or 6 Ma as suggested by subsidence analysis, the resulting amount of incision should be comprised between 500 m and 600 m which is in the same order of magnitude than what we have calculated here (387 ± 105 m).

We suggest that the following scenario from the Early Miocene to the present occurred: during the Early Miocene faulting, deformation and uplift of the Koralpe and Pohorje mountains occurred (Fig. 1.10). During the quiet Middle Miocene period we suggest that the relict landscape were created probably by smoothing and possibly decay (lowering of elevation) of the topography created during the Early Miocene. While the Drava remained at constant elevation, the rivers connected to the Drava started to incise and record the surface uplift of Koralpe and Pohorje (Fig. 1.10, 1.11). Then, the Koralpe and Pohorje Mountains, as well as the surrounding sedimentary basins were uplifted together in a renewed uplift event that started at the end of Miocene and involved some 400 m of surface uplift since then for Koralpe and Pohorje. We cannot rule out other, more complex scenarios, but we argue that to

explain the described morphology and taking in account all available indirect constraints, the scenario proposed here is currently the simplest.

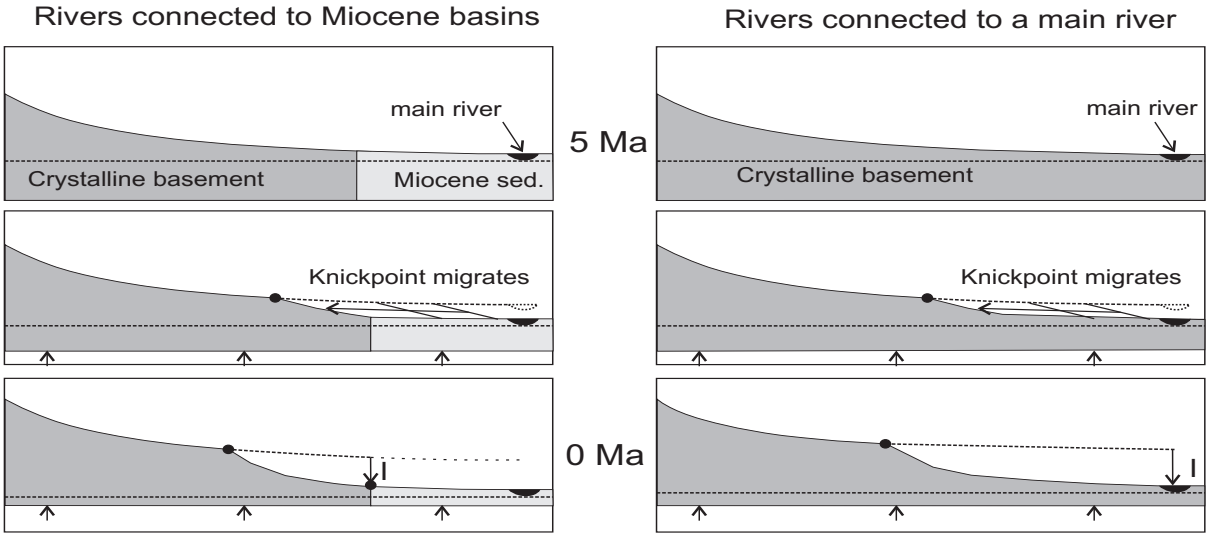

Figure 11
Legrain et al., 2013

Figure 1.11: Schematic channel profiles through different time steps during the incision into the Koralpe and Pohorje relict landscapes. *I* refer to Incision amount.

Our interpretations partly contradict previous work and we explain in the following why we think that our interpretations are more consistent based on our results. For example, Frisch et al. (2000) interpreted the Koralpe ´paleosurface´ to be of Oligocene age. This is contradicted be our morphometric analysis and in particular by the fact that the relict landscape is also present on the Western slope of the Koralpe tilted block. We explain this contradiction by the fact that we have used here new methods in term of morphometric analysis that allowed us to make more precise interpretations on the possible age of the relict landscape. Our results also contradicts the idea of a surface uplift of the Koralpe Mountain of more than 800 m since the late Miocene as it has been suggested based on occurrence of gravels on top of the Koralpe ´paleosurface´ (Pischinger et al., 2008; Kurz et al., 2011). We rather suggest a surface uplift of around 400 m based on the channel profile analysis. Our results also clearly contradict the interpretation that the Koralpe Rivers are well equilibrated and do not features significant knickpoint other than lithological (Rantitsch et al., 2009). Our analysis of the Koralpe channels and hillslopes is very hard to combine with this interpretation (Fig. 1.3, 1.4, 1.6, and 1.7) and we argue that Rantitsch et al. (2009) did not correctly fit the different channels segments of the Koralpe rivers and therefore misinterpreted the Koralpe landscape as being

well equilibrated. Despite the contradictions listed above with the literature that we attribute to the fact that our morphometric analysis provides a more quantitative description of the Koralpe and Pohorje relict landscapes than before, a significant part of our interpretations in fact support previous work. Our results are in line with the following interpretations: (1) most of the Koralpe landscape is a relict landscape (Winkler-Hermaden, 1957; Frisch et al., 2000), (2) The Koralpe mountain can be considered as an eastward tilted block (Genser and Neubauer, 1990; Frisch et al., 2000; Kurz et al., 2011) and (3) the exhumation of the Pohorje granite was extremely fast and related to tectonic denudation due to the early Miocene extension (Sachsenhofer et al., 1998; Fodor et al., 2008).

1.6. Conclusion

We can draw several conclusions concerning the landscape evolution of the never glaciated Koralpe and Pohorje mountains:

- The Koralpe and Pohorje mountains show strong evidences of transient erosion based on hillslopes and channel profiles analysis. Their landscapes can be divided in an upper relict landscape, and lower incised landscape.

- The Koralpe and Pohorje relict landscapes are younger than 16-15 Ma as indicated by the exhumation of the Pohorje granite and the extent of the relict landscape on both sides of the tilted Koralpe block. This exclude the possibility that these relict landscapes represent older (Pre-Miocene) deformed relict landscapes.

- The incision into the two relict landscapes averages 383 m ± 105 m and is probably the result of an increased rock uplift rate since the last Miocene (6-5 Ma) affecting the studied mountains and the surrounding Miocene basins.

- The Koralpe and Pohorje relict landscapes were most likely created during the late Miocene, between 16-15 Ma and 5 Ma, a period of tectonic quiescence that allowed the topography to decay and become smoother.

Chapter 2

Landscape Rejuvenation and Post-Miocene Increase in Rock Uplift Rate at the Eastern End of the Alps

Abstract

In the ongoing debate on the landscape evolution of the Alps, most of the recent studies have focused on heavily glaciated areas during the last periodic glaciations and resulting climatically-driven uplift and erosion processes. Here we present ^{10}Be-derived erosion rates from a region of the Alps that was never glaciated: the Koralpe Mountain, at the eastern end of the Alps. This region features strong geomorphological evidences of landscape transience with incised valleys into a smooth relict landscape. Erosion rates average 49 ± 8 m/Ma for catchments located on the relict landscape, above the knickpoints, and 137 ± 15 m/Ma for catchments in the incised landscape, below the knickpoints. Small catchments (< 6 km²) comprising both relict and incised landscape are interpreted as random values between the two end-member erosion signals because of poor sediment mixing in the channels. We calculate an estimation of onset of incision at 4 ± 1 Ma, an estimation of surface uplift of 349 ± 92 m, and a total relative base level fall of 543 ± 143 m. Our results are in close agreement with both the magnitude and the age of onset of uplift of the Styrian Basin and the North Molasse Basin, as well as the incision rate of the Mur River into the Styrian Karst. We suggest that the whole area is experiencing the same post-Miocene increased rock uplift, possibly in response to a deep-seated process such as delamination of the lithosphere below the Alps. Our results are important because they show a clear signature of a tectonic related uplift on erosion rates, at the eastern end of the Alps, recorded in the form of an ongoing wave of incision.

2.1. Introduction

The recent topographic evolution of the European Alps and its relationship with climate and tectonics remains strongly debated. Although at global scale the significant increase in erosion rate since the late Miocene may only be apparent (Willenbring and von Blanckenburg, 2010), at the scale of the Alps, different datasets support the view of an increase in erosion and presumably in uplift since the late Miocene. While this post-Miocene increase in erosion and uplift in the Alps is relatively well documented, the tectonic and/or climatic driving mechanisms responsible for this increase are still a matter of debate (Dunkl et al., 2005; Wagner et al., 2010, Hergarten et al., 2010; Willett, 2010, Delunel et al., 2010, Persaud and Pfiffner, 2004; Wittmann et al., 2007; Khulemann et al. 2002; Champagnac et al., 2007; Campani et al., 2012). Recent studies suggest that a significant part of the post-Miocene rock uplift and erosion increase in the Swiss Alps can be attributed to Plio-Pleistocene glacial carving and resulting erosion-driven uplift (Champagnac et al., 2007; Valla et al., 2011; Sternai et al., 2012) and to long-term landscape transience due to the repeated glacial-interglacial cycles (Norton et al., 2010a).

However, a tectonic component in the recent uplift pattern of the Alps is still not excluded, either in the form of convergence and crustal thickening, especially in the Eastern Alps, or in the form of deep-seated processes such as slab break-off or delamination of the lithosphere that could have modified the isostatic equilibrium of the Alpine orogen. Most of the Alps, except the Eastern Alps, experience no measurable convergence at present (Bus et al., 2009) but other tectonic processes than active convergence and crustal thickening could have contributed to the increase in erosion in the Alps since the late Miocene. For example, deep-seated processes such as delamination of the lithosphere or slab break-off could also partly explain the increase in erosion of the Alps since the late Miocene (Genser et al., 2007).

Although interesting, this hypothesis seriously lacks quantitative constraints on the timing and magnitude of increase in rock uplift in the Alps from regions where climate related erosion and uplift increase can be excluded. The Koralpe Mountain is located at the eastern end of the Alps and has largely escaped glacial carving during the last glacial maximum (LGM). This fluvial landscape, already interpreted as an incised relict landscape probably of Miocene age (Chapter 1), represents a good opportunity to test the hypothesis of a tectonic component in the post-Miocene erosion and rock uplift increase in the Alps.

First, we present ^{10}Be-derived erosion rates from the relict and incised landscape of the Koralpe Mountain in order to test the hypothesis of the Koralpe Mountain as a transient, incised relict landscape (Chapter 1). Then, we use the ^{10}Be-derived erosion for the two parts of the landscape and the known amount of incision into the relict landscape (Chapter 1) to calculate an estimation of the age of onset of incision and an estimation of the amount of total relative base level fall since onset of incision. We compare these results with different datasets from surrounding regions to explore what tectonic or climatic changes may explain the observed post-Miocene rock uplift increase in this part of the Alps. Finally, we suggest an estimation of topographic evolution for the Koralpe Mountain since the late Miocene and we compare it with the recent topographic of the rest of the Alps.

.

2.2. Geological setting

The Koralpe Mountain is located at the eastern end of the Alps, at the transition with the Pannonian basin. It is bordered to the west by the Lavanttal Fault, one of the major strike-slip faults that had its peak of dextral strike slip activity in the Early Miocene, during the lateral extrusion of the Eastern Alps (Ratschbacher et al., 1991; Frisch et al., 1998). The fault is a conjugate couple to the sinistral Mur-Mürz fault and the two delineate the Styrian Block to their East (Wagner et al., 2011). Apatite fission track and (U-Th)/He thermochronology from the Koralpe Mountain suggest a relatively steady exhumation since the Eocene of ~ 100 m/Ma (Chapter 1; Hejl, 1997). During the Early Miocene, the Koralpe Mountain is interpreted to have been tilted eastwards with the tilting having occurred during the main activity of the Lavanttal fault: between 18 Ma and 16 Ma (Neubauer and Genser, 1990; Kurz et al., 2011; Chapter 1).

Lithologically, the Koralpe Mountain is composed of paragneisses eclogites and mylonitic gneiss that were metamorphosed during the Eoalpine orogeny some 90 Ma ago (Tenczer and Stüwe, 2003). The area also comprises small marble lenses (< 500 m length) that only represent a small part of the Koralpe Mountain. Overall, except the very small marble lenses, all the Koralpe rocks are very quartz rich and allow for ^{10}Be-derived erosion rates sampling in all location of the Koralpe Mountain. Morphologically, the Koralpe region is characterized by two different areas: the smooth relict landscape and the steeper incised landscape (Chapter 1) but relict landscapes have long been documented in the Koralpe Mountain (Winkler-

Hermaden 1957; Frisch et al. 2000). Channel profile projection of six channels from the Koralpe Mountain indicates an average total amount of incision of ~ 350 m into the relict landscape (Chapter 1). The mean annual precipitation of Koralpe scale with elevation and range from 900 mm/y at the lowest elevations to 1600 mm/y in the summit area.

2.3. Methods

2.3.1. Morphometric analysis and definition of variables for vertical movements

While the morphometric analysis performed in Chapter 1 was based on the SRTM 90 m resolution DEM, we have used here a 10 m resolution DEM that is available for the Koralpe Mountain and the Styrian Basin. The higher resolution neither significantly changes the mapping of the relict landscape nor the calculated amount of incision calculated from channel profile projection (Chapter 1) because the mapped relict landscape and the channel profile are features significantly larger than the DEM resolution of 90 m or 10 m. The only advantage of using the 10 m DEM is the more detailed calculation of hillslopes gradient, especially at small scale and for very small catchments that we have sampled for ^{10}Be-derived erosion rates.

When a step increase in rock uplift occurs, from an initial rock uplift rate U_i to a final rock uplift rate U_f, channels adjust by incision and the incised part of the landscape erode at a similar rate than the new uplift rate (U_f) while the relict landscape is still eroding at the same rate than the initial rock uplift rate (U_i) (Fig. 2.1; Kirby and Whipple, 2012). When U_i, U_f, and the amount of incision Δz are known, it is possible to calculate the time needed for the incision (Whipple and Tucker, 1999; Kirby and Whipple, 2012; Miller et al., 2013):

$$\Delta t_k = \Delta z / (U_f - U_i) \quad (2.1)$$

The total relative base level fall (ΔB_k) can be calculated by adding the amount of erosion of the relict landscape since the beginning of uplift to the measured incision amount of incision from channel projection (Whipple and Tucker, 1999; Kirby and Whipple, 2012; Miller et al., 2013):

$$\Delta B_k = \Delta z + (U_i \Delta t_k) \quad (2.2)$$

Based on the results of channel projection of the Koralpe Mountain (Chapter 1) and the equations 2.1 and 2.2, we use a simple uplift model for the Koralpe region that to define what represent the different vertical motion (rock uplift, surface uplift, erosion) between different areas and different methods that we discuss in this paper (Fig. 2.1). Indeed, we want to compare the incision of the Koralpe relict landscape with three other datasets: the incision record of the Mur River in the Styrian Karst measured from burial age dating of cave sediments (Wagner et al., 2010), subsidence analysis of the Styrian Basin (Ebner and Sachsenhofer, 1995; Sachsenhofer et al., 1998), and subsidence analysis of the North Molasse Basin (Genser et al. 2007). For Koralpe, Δz represents the amount of incision since the rock uplift increase and ΔB_k is the total amount of base level since the onset of uplift, also equivalent to the total amount of rock uplift since the uplift increase (Fig. 2.1). Subsidence analysis records rock uplift of the bottom of the basin and is therefore a proxy of rock uplift. The total amount of rock uplift is thus equivalent to the total relative base level fall (ΔB_{bs} and ΔB_{bn} for the Styrian Basin and the North Molasse Basin respectively)

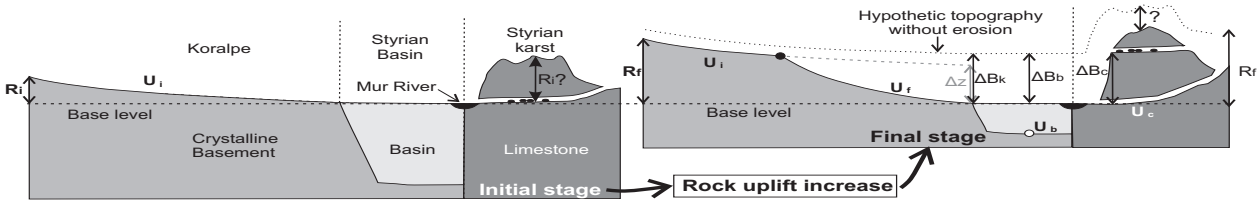

Figure 7
Legrain et al., 2013b

Figure 2.1: Synthetic cross-section showing a simplified model of uplift of the studied region with definition of variables. Note that the scale is not respected especially between R_f and R_i for Koralpe.

The methods discussed above can give direct constraints on surface uplift and topographic evolution. Subsidence analysis records rock uplift of the bottom of the basin and does not give direct constraints on surface uplift. It is not evident if dating of cave sediments can directly measure surface uplift. Sediments in cave can only be dated by cosmogenic isotopes if buried at sufficient depths below the surface to ensure complete shielding which implies that there is a part of the topographic relief higher than the dated cave. This is problematic to infer surface uplift because the initial relief R_i cannot be deduced by using the final relief R_f and the age of the dated sediments. Indeed, the amount of erosion of the topography that takes place above the highest cave level is unknown (Fig. 2.1). Therefore, even if ΔB_c gives an idea of the order of magnitude of the amount of surface uplift that took place since the rock uplift increase, this method does not allow for an explicit calculation of this amount. Of the three methods, only the amount of incision Δz calculated from channel profile projection is therefore giving some

direct quantitative constraints on surface uplift of the region since the increase in rock uplift rate.

2.3.2. ^{10}Be-derived erosion rates

Erosion rates averaged over 10^3 to 10^5 years timescale can be calculated from *in-situ* produced cosmogenic nuclides, ^{10}Be in quartz being the most used and the best calibrated method (Brown et al., 1995; Bierman and Steig, 1996, Granger et al., 1996; Schaller et al., 2001, von Blanckenburg, 2006). The measured concentration (C) of ^{10}Be in quartz is inversely proportional to erosion rates (ε) and can be expressed as (Brown et al. 1995, von Blanckenburg, 2006):

$$C = P_c / (\varepsilon \lambda) \tag{2.3}$$

where P_c is the mean catchment production rate and λ is the attenuation length of particles that contributes to the production. For some of the sampled catchments, we have also calculated erosion rates of nested catchments following for the incised part of the landscape (Reinhardt et al. 2007):

$$\varepsilon_i = (\varepsilon_e A_e - \varepsilon_r A_r) / A_i \tag{2.4}$$

where ε is erosion rate and A drainage area of the catchment, and the subscripts i, e and r refer to entire catchment, incised part of the catchment and relict part of the catchment respectively. To extract the erosion signal of the relict and incised parts of the Koralpe Mountain we have taken samples for cosmogenic ^{10}Be-derived erosion rates from both parts of the landscape. The samples can be divided into four categories based on their extent relative to the incised relict landscape described in Chapter 1: "*relict*", "*incised*", "*mixed*" and "*glaciated*". *Relict* and *incised* categories refer to catchments entirely located within these morphometric regions and *mixed* landscape refers to catchments comprising both incised and relict parts of the landscape to various extents within their drainage areas. The category *glaciated* refers to catchments that were entirely or partly glaciated during the LGM.

In addition to these categories we also define another classification based on the drainage area of the sampled catchments. Indeed, most of the catchments that we have sampled are very

small and it is important to determine if the sampled catchments mostly reflect hillslopes or fluvial processes. Based on channel profile analysis and slope-area plots (Chapter 1), we found that the critical drainage area (A_{cr}) for the Koralpe Mountain is usually comprised between 1 km² and 7 km². As a conservative value we define the transition between hillslopes and fluvial catchment to be around 7 km² for the Koralpe Mountain. Based on these results from DEM analysis, we define three categories based on drainage area of the catchments: "*bedrock sample"* (A = 0), "*hillslopes"* catchments (A < 7 km²) and "*fluvial" catchments* (A > 7 km²).

The term *hillslope* catchment seems contradictory but, in theory, even though the small catchments are almost entirely controlled by hillslope processes the sampled sand at the outlet of the small catchment still collect and average the erosion signal of the entire small catchment. However, in practice, it is not clear if these small catchments can give an accurate average erosion rate of the entire catchment. Indeed, appropriate mixing of sediments in the stream is necessary to calculate an accurate average erosion rate for the entire catchment. In these very small catchments it is very likely that sediments are very poorly mixed. We therefore take in account this potential bias in this study by a careful analysis of the results compared to the drainage area of the catchments. Combining both classifications, our ^{10}Be-derived erosion rate samples can be divided into six categories (Fig. 2.2, Table 2.2): (1) *relict hillslope*, (2) *mixed hillslope* (3) *mixed fluvial* (4) *incised hillslope* (5) *relict bedrock* and (6) *glaciated hillslope.*

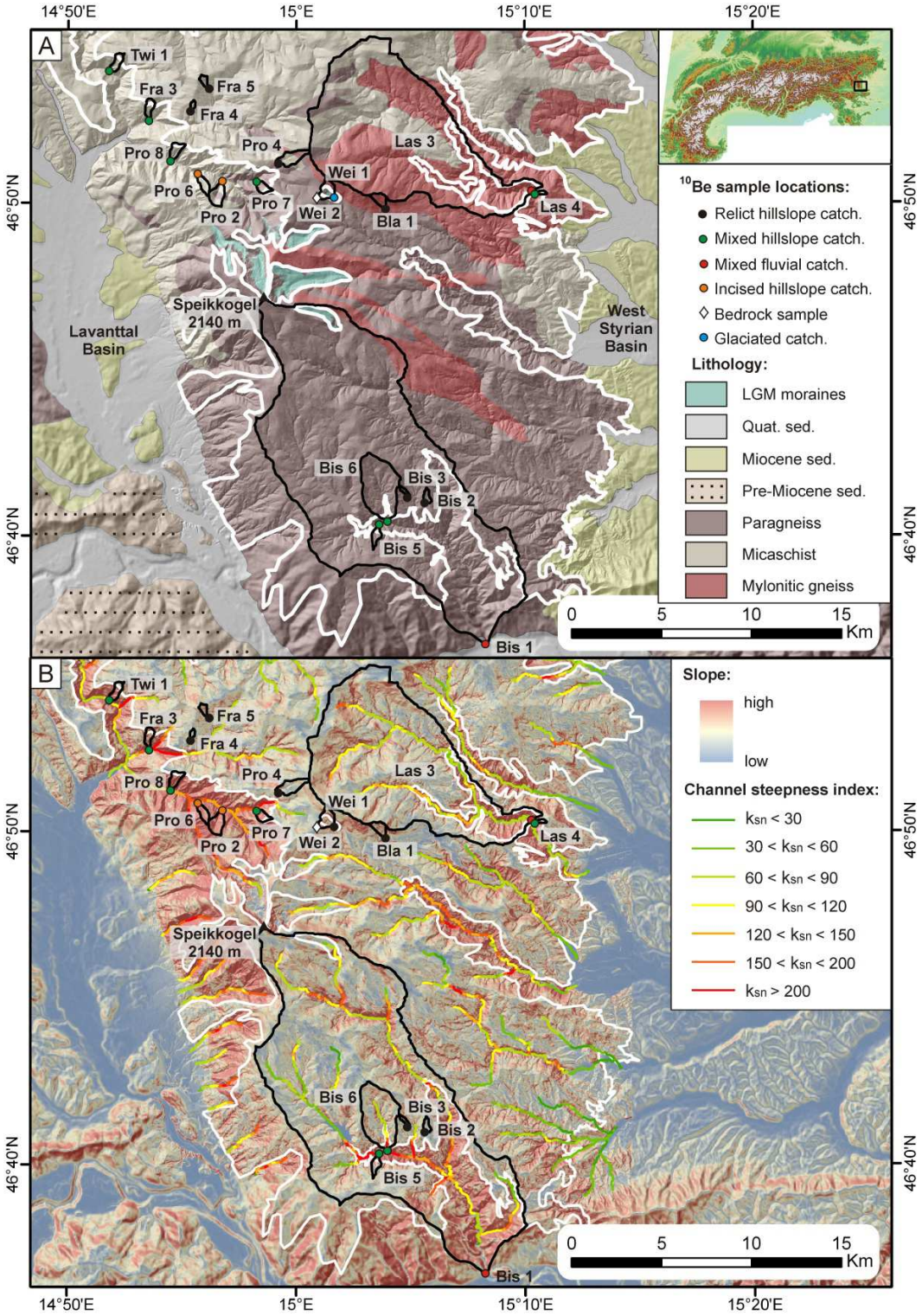

Figure 2.2: Map of the Koralpe Mountain with location of the ^{10}Be samples. Thick white line is the extent of the relict landscape (Chapter 1). A: Location of the samples and simplified lithological map of Koralpe. The southern part of Koralpe mainly consists of paragneisses while the northern part mainly features micaschists. On the eastern side of Koralpe is also present mylonitic gneiss (the so-called "Plattengneiss"). B: Spatial variations in slope and channel steepness index calculated from a 10 m resolution DEM. Normalized channel steepness index was calculated with a reference concavity index of 0.45 and over 500 m segments for all channels with $A >$ 1 km^2.

2.4. Results

^{10}Be-derived erosion rates from the Koralpe Mountain range from 36 m/Ma to 149 m/Ma. They are consistent with the long-term exhumation rate inferred from thermochronology for the Koralpe Mountain of ~ 100 m/Ma since the Eocene (Hejl, 1997; Chapter 1). Koralpe erosion rates are one order of magnitude lower than ^{10}Be-derived erosion rates from the Western, Central, and Eastern Alps that where glaciated during LGM typically around 1000 m/Ma (Delunel et al., 2010; Whittman et al., 2007; Norton et al., 2010b; Norton et al., 2011). However, despite the significantly lower erosion rates, Koralpe erosion rates show a clear difference between relict and incised landscape. Indeed the mean erosion rate of the incised catchments is more than 2.5 higher than the mean erosion rate of the relict landscape (137 ± 15 m/Ma and 49 ± 8 m/Ma respectively, Table 2.1). Erosion rates from the Koralpe relict landscape show little variability and range from 36 ± 3 m/Ma to 59 ± 4 m/Ma (Table 2.1). Similarly, the two entirely incised catchments erosion rates are very consistent: Pro-6 = 111 ± 9 m/Ma and Pro-2 = 149 ± 14 m/Ma. Erosion rates of catchments comprising both incised and relict landscape average 81 ± 24 m/Ma and show more variability: they range from 56 ± 3 m/Ma to 123 ± 9 m/Ma. In addition to the erosion rates from the Koralpe Mountain, we have measured erosion rates from three catchments located in the Styrian Basin, East of the Koralpe Mountain. These erosion rates range from 33 ± 2 m/Ma to 123 ± 9 m/Ma (Table 2.1). The two larger catchment (Sti-1 and Pic-1) are consistent while the small catchment Sau-1 show a very low erosion rate of 33 ± 2 m/Ma. The erosion rates from the Styrian Basin are relatively high and average 88 ± 40 m/Ma (Table 2.1).

Table 2.1: Morphometric parameters and calculated ^{10}Be-derived erosion rates of the sampled catchments

Sample	Long. (°)	Lat. (°)	Elevation (m)	Area (km²)	Slope[a] (°)	Fraction Incised[b]	Sample weight (g)	^{10}Be concentration ($x10^4$ at/$g_{(Quartz)}$)	Topographic shielding factor[c]	Snow shielding factor[c]	Mean production rate[d] (at/g/yr)	Apparent age[e] (yr)	Erosion rate[f] (m/Ma)	E^* [g] (m/Ma)
Glaciated														
Wei-1	15.026	46.335	1447	0.71	21.2	-	29.38	15.06 ± 0.80	0.98	0.89	18.14	6742	89 ± 6	-
Relict landscape														
Wei-2	15.015	46.836	1722	-	-	-	28.09	37.62 ± 2.31	1.00	0.89	19.05	16667	36 ± 3	-
Fra-4	14.922	46.880	1084	0.11	12.7	0.00	26.89	20.00 ± 0.91	1.00	0.93	12.18	12766	47 ± 3	-
Fra-5	14.934	46.890	1193	0.21	17.2	0.00	28.72	19.00 ± 0.87	0.99	0.92	13.88	10909	55 ± 3	-
Pro-4	14.987	46.852	1476	0.91	12.9	0.00	32.58	34.46 ± 1.32	1.00	0.90	17.26	16667	36 ± 2	-
Bla-1	15.063	46.831	1451	0.46	21.0	0.00	28.03	19.45 ± 0.93	0.98	0.91	15.49	10169	59 ± 4	-
Bis-2	15.092	46.683	1047	0.24	10.3	0.00	28.73	19.00 ± 0.93	1.00	0.94	11.59	12766	47 ± 3	-
Bis-3	15.081	46.686	1070	0.14	15.1	0.00	29.36	17.98 ± 0.80	1.00	0.93	11.85	11765	51 ± 3	-
					14.9 ± 3.4								**49 ± 8** [h]	
Mixed landscape														
Twi-1	14.862	46.899	556	0.45	23.3	0.74	27.77	8.72 ± 0.47	0.98	0.95	9.60	6742	89 ± 6	109 ± 7
Fra-3	14.891	46.874	577	0.40	24.6	0.71	30.25	14.05 ± 0.66	0.97	0.95	9.91	10714	56 ± 3	107 ± 7
Pro-7	14.971	46.844	1107	0.37	26.8	0.81	40.47	8.95 ± 0.54	0.97	0.91	14.49	4878	123 ± 9	115 ±8
Pro-8	14.908	46.854	623	0.48	27.6	0.86	40.48	12.75 ± 0.57	0.96	0.95	10.13	9524	63 ± 4	118 ± 8
Las-4	15.173	46.838	701	0.10	28.3	0.66	29.84	9.78 ± 0.49	0.97	0.97	8.23	8696	69 ± 4	102 ± 6
Bis-5	15.060	46.672	758	0.39	17.7	0.42	33.06	7.50 ± 0.45	0.99	0.94	11.06	5128	117 ± 8	83 ± 6
Bis-6	15.066	46.673	734	5.84	16.9	0.05	40.24	11.70 ± 1.11	0.99	0.93	12.45	7317	82 ± 9	53 ± 6
Bis-1	15.139	46.613	382	142	17.9	0.17	30.25	11.74 ± 0.87	0.99	0.92	11.70	8696	69 ± 6	63 ± 5
Las-3	15.173	46.838	542	66	18.6	0.12	31.65	13.70 ± 0.60	0.99	0.92	12.08	9836	61 ± 4	59 ± 3
					22.4 ± 4.4	**0.51**							**81 ± 24**	
Incised landscape														
Pro-2	14.945	46.844	866	0.81	27.8	1.00	30.31	6.72 ± 0.58	0.97	0.93	12.91	4027	149 ± 14	-
Pro-6	14.927	46.848	737	0.45	29.4	1.00	40.78	8.24 ± 0.61	0.96	0.94	11.68	5405	111 ± 9	-
*Bis-1**	-	-	-	*30*	*28.0*	*1.00*	-	-	-	-	-	*4110*	*146 ±7*	-
*Las-3**	-	-	-	*8.19*	*27.7*	*1.00*	-	-	-	-	-	*4196*	*143 ±4*	-
					28.2 ± 0.7								**137 ± 15**	
Styrian Basin														
Sti-1	15.591	49.905	304	68	9.3	-	31.23	4.35 ± 0.31	0.99	1.00	6.36	4878	123 ± 9	-
Pic-1	15.750	47.003	326	28	10.4	-	30.70	4.91 ± 0.38	1.00	0.99	6.40	5454	110 ± 9	-
Sau-1	15.311	46.842	317	6.60	5. 9	-	40.14	15.47 ± 0.86	1.00	0.99	6.09	18182	33 ± 2	-
					8.5 ± 1.9								**88 ± 40**	

Bold numbers are average of the above values with standard deviation around the mean
a Mean slope of the catchments calculated from the 10 m resolution DEM
b Fraction of incised landscape within the catchment.
c Snow shielding correction was calculated from the annual Swiss snow data (Aauer 2003) and topographic shielding was calculated from the 10 m DEM.
d Production rates include topographic and snow shielding
e Apparent ages are calculated as the time to erode ~ 60 cm of bedrock (considering a density of 2.7 $g.cm^{-3}$)
f Erosion rates were calculated using the scaling laws of Dunai (2000) and production equations of Schaller et al. (2002)
g E^* is calculated based on their fraction of incised landscape and a simple mixing model between the relict and incised landscapes erosion rates (refer to text for more details)
h Erosion rate of the bedrock sample (Wei-2) is not included in the mean erosion rate of the relict landscape catchments.

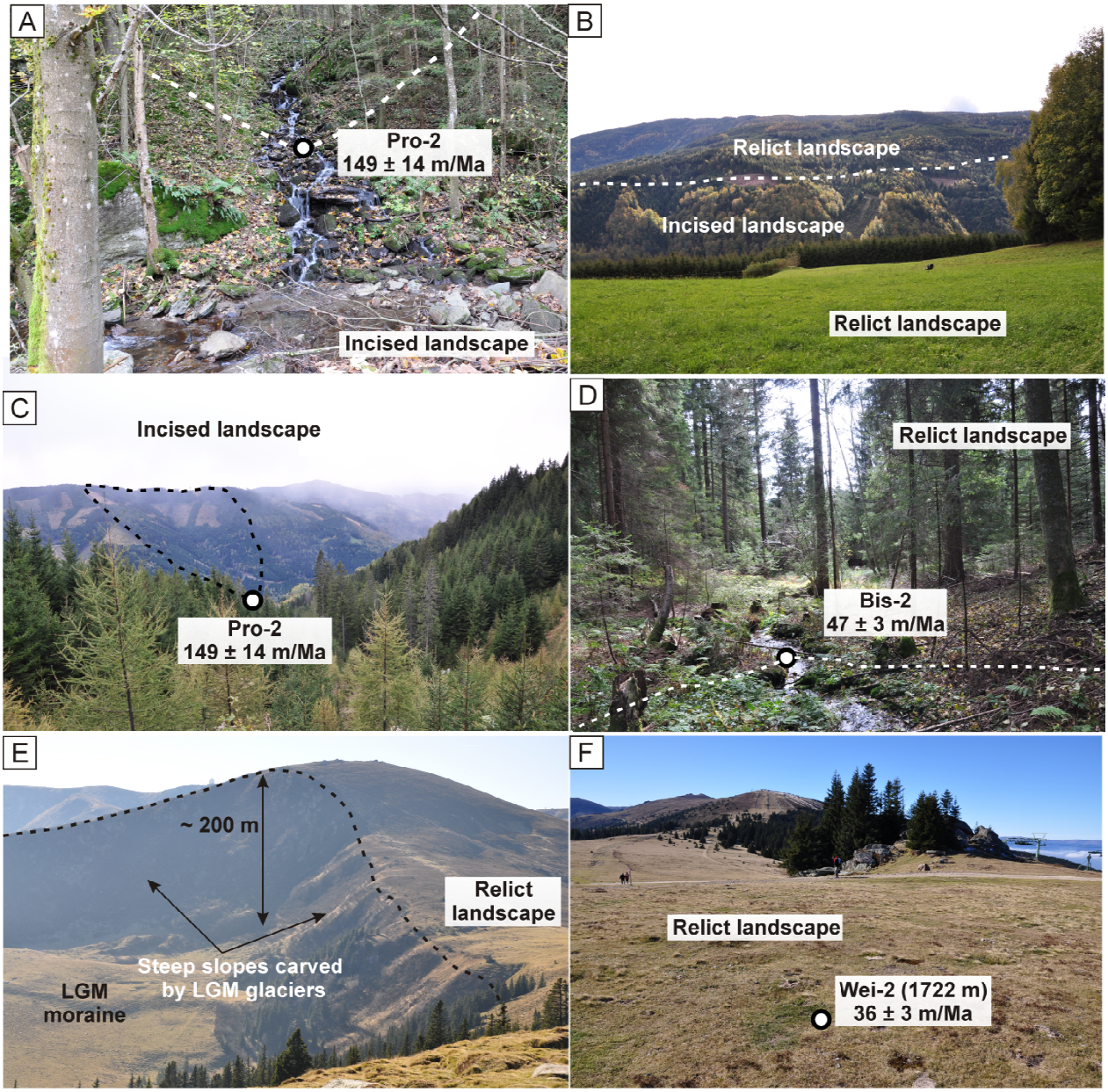

Figure 2.3: Photographs from the Koralpe Mountain. A: Sampling location of the highest erosion rate in the incised landscape of Koralpe, trunk stream in the foreground (Prössingbach River) flows from left to right. B: View to the South in the Bistrica catchment, approximately from the sampling location of Bis-3; Break-in-slope separates the low slope relict landscape from the steeper incised landscape below. C: View of the entire catchment Pro-2 showing the steeper slope of the incised landscape (compare to photographs D and F). D: View looking downstream of the sampling location of Bis-2 showing the gentle slopes of the Koralpe relict landscape hillslopes. E: View looking south showing a glacier cirque carved by a 3 km long LGM glacier (See Fig. 2.4 for location of the cirque). F: View to the South of the very smooth crest of the Koralpe Mountain forming part of the relict landscape.

2.4.1. LGM glacial overprint on the relict landscape around the Koralpe summit

Even if the LGM glaciers did not cover a large area of the Koralpe landscape (Fig. 2.1), it is important to analyze their impact on the morphology to avoid any confusion between fluvial and glacial incised valleys and steepened hillslopes. The LGM glaciers were restricted to the Koralpe summit region, around the Grosse Speikkogel (2140 m), and were < 5 km long (Fig. 2.4). However, these small glaciers have significantly disrupted the smooth surface of the relict landscape and created glacier cirques with very steep faces of up to 200 m height (Fig. 2.3E, 2.4). We have only measured one erosion rate from the glacially influenced landscape but this rate (Wei-1: 89 ± 6 m/Ma) is almost two times higher than the average erosion rates of the catchments located on the relict landscapes but not glacially influenced (49 ± 7 m/Ma). The mean slope of the catchment Wei-1 (21.2°), glaciated during the LGM, is very similar to the mean slope of the never glaciated catchment Bla-1 (21.0°). However, the erosion rate of the catchment Wei-1 (89 ± 6 m/Ma) is significantly higher than the erosion rate of the catchment Bla-1 (59 ± 4 m/Ma). This difference in erosion rate, despite similar mean slope, could be explained by the occurrence of very steep slopes left by the LGM glaciers in the Wei-1catchment.

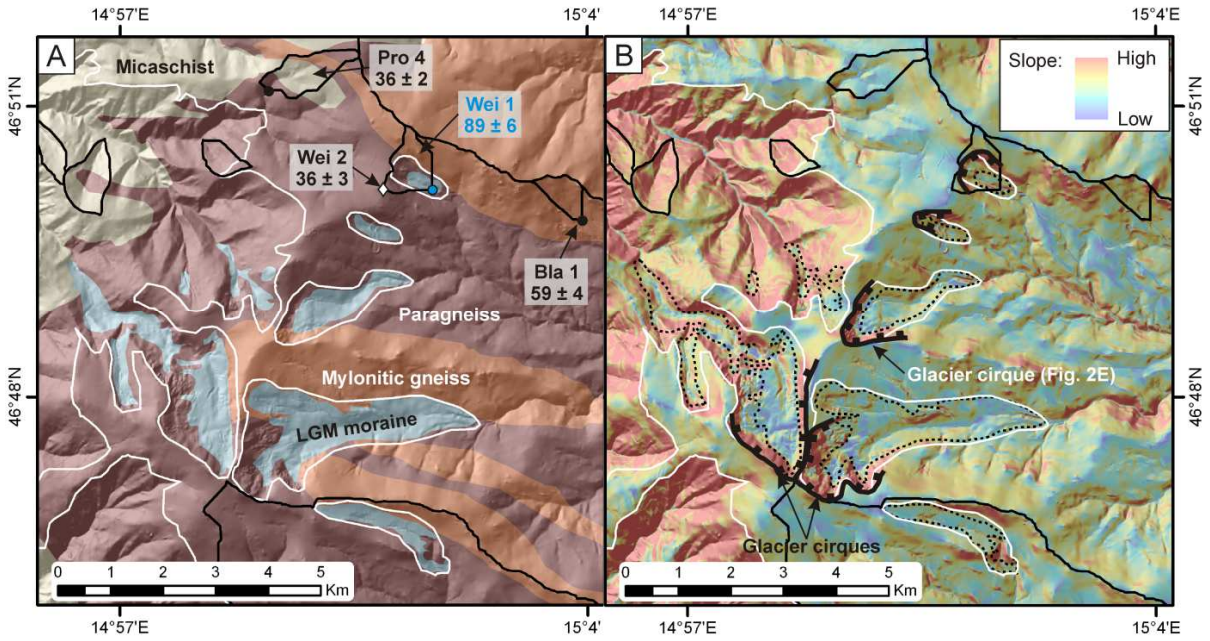

Figure 2.4: Glacial overprint on the upper part of the relict landscape. A: Lithology, extent of the LGM moraines and measured erosion rates from the relict landscape in the upper part of the Koralpe Mountain, white line show the extent of the relict landscape. B: Slope map and location of glacier cirques carved by LGM glaciers, dashed black line shows the extent of LGM moraines.

Such glacial influence on present day erosion rate seems very interesting to study in further details but we are only interested in this study in non-glacial transient landscape. Because the influence of the LGM glaciers on the Koralpe morphology is very obvious in term of erosion rates, slope, and glacial moraine deposits (Fig. 2.3), we can clearly exclude any confusion between disruption of the Koralpe relict landscape by glaciers during the past glaciations, and fluvial incision into the Koralpe relict landscape.

2.4.2. Relationships between erosion rates and morphometric parameters

Koralpe erosion rates show a good correlation with mean catchment slope and the data can best be fitted by a non-linear model (Montgomery and Brandon, 2002) with a critical slope (S_c) of 35°, consistent with other non-glaciated mountain ranges in the world (Fig. 2.5A; Ouimet et al., 2009; Dibiase et al., 2010; Carretier et al., 2012). The *relict* and *incised* samples show a very good fit with this model while *mixed hillslope* samples catchments show more scatter, with some samples featuring high slope and low erosion rate and others low slope and high erosion rate (Fig. 2.5A). Koralpe erosion rates show a moderate positive linear correlation with the fraction of incised landscape within their catchment (r^2 = 0.49; Fig. 2.5B). Similar to the plot of erosion rates versus slope, the samples from the *mixed hillslope* catchments show a large scatter: the coefficient correlation omitting the *mixed hillslope* catchments is significantly better (r^2 = 0.90; n = 10) than the correlation coefficient for all the data (r^2 = 0.49; n = 17). In fact, the *mixed hillslope* catchments alone show no correlation at all with the fraction of incised landscape (r^2 = 0.02) and add a significant scatter to the data. Interestingly, the *mixed fluvial* catchments are very consistent with the linear fit. The very small size of the catchments and potential inappropriate mixing of the stream sediment at the sampling location could explain the absence of correlation of the *mixed hillslope* catchments.

To test this hypothesis, we have calculated for each *mixed fluvial* and *mixed hillslope* catchment a theoretical erosion rates (E^*) based on the best linear fit between the two end-members erosion signal of the *relict* and *incised* catchments. This theoretical erosion rate is calculated as $E^* = 81\ f + 49$, where E^* is the calculated erosion rate, and f is the fraction of incised landscape within the catchment (Fig. 2.5; Table 2.1). The two end-members erosion signal are thus taken as the average erosion rate of all the *incised* catchments (n = 2; 130 m/Ma) and *relict* catchments (n = 6; 49 m/Ma). Ideally mixed samples between the two end-

members erosion signal should have a similar measured and calculated erosion rate ($E/E^* = 1$). We have plotted this ratio between calculated and measured erosion rate against drainage area of the catchments (Fig. 2.5C). Only three samples show a ratio of 1 within errors. One of these catchments is Pro-7 but at the same drainage area all other samples are very scattered which is suggesting no relationship, at this drainage area, between calculated and measured erosion rates. In contrast, the two largest *mixed fluvial* catchments (Bis-1 and Las-3) show a good match between calculated and measured erosion rate. This result is consistent with the idea of a threshold of minimum drainage area of the catchment where sediments in the streams start to be correctly mixed and thus provide a good average of the erosion of the catchment.

The mixing threshold drainage area between correctly mixed sediments and incorrectly mixed sediments would fall between the drainage area of the sample Bis-6 (5.8 km²) and the drainage area of the sample Las-3 (66 km²).Interestingly the critical drainage area A_{cr} for Koralpe is usually comprised between 1 and 7 km². There is a good match between the transition between hillslopes and channels derived from the DEM and the sediment mixing threshold suggested by the erosion rates. Although as small as the mixed hillslope catchments, the *incised hillslope* and *relict hillslope* catchments seem very consistent and not affected by this bias. This could be explained by their spatial homogeneity in term of slope and thus probably also in term of erosion rate: even if the sampled sand was poorly mixed, the calculated erosion rate still yields an accurate average erosion rate of the whole catchment.

Because of this inappropriate sediment mixing of the mixed hillslopes catchments samples we have only deconvolved the erosion rate of the incised part for the two mixed fluvial (Bis-1 and Las-3) with equation (2.4). The calculated erosion rates (Bis-1* = 146 ± 7 m/Ma and Las-3* = 143 ± 8 m/Ma) are very consistent with the two erosion rates of the small catchments entirely located in the incised landscape (Table 2.1, Pro-6 = 111 ± 9 m/Ma and Pro-2 = 149 ±14 m/Ma). It is important to note that these two types of erosion rates are independent from each other because we did not use the erosion rates of the small incised catchments for calculating the erosion rates of Bis-1* and Las-3*. We therefore take as the representative erosion rate of the incised landscape of Koralpe the average of these four erosion rates (137 ± 15 m/Ma).

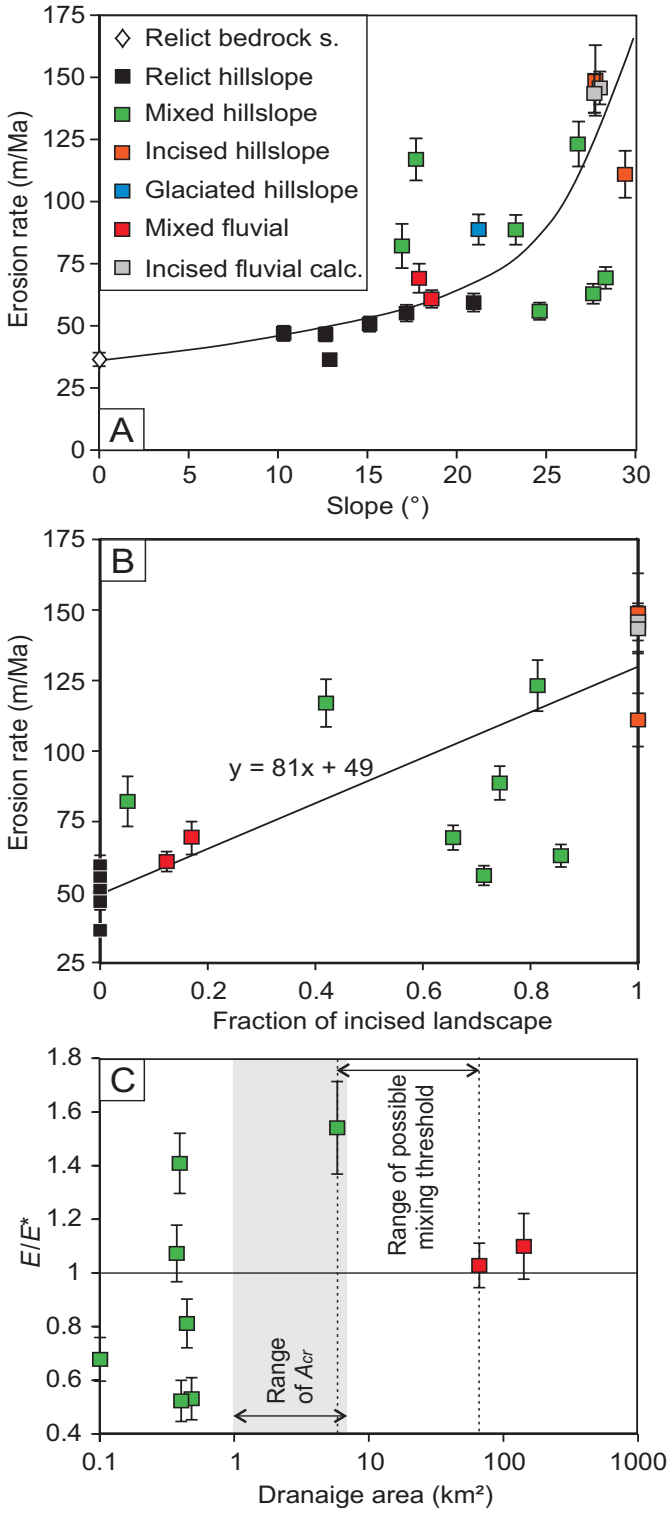

Figure 3
Legrain et al., 2013b

Figure 2.5: Plots of erosion rates versus different geomorphic parameters. A: Erosion rates versus mean slope of the catchments, black line is a fit of the data with a non-linear model: $E = E_0 + KS/(1 - S/S_c)$ (Montgomery and Brandon, 2002) K = 0.035 mm/y and background erosion rate (E_0) of 36 m/Ma (sample Wei-2). B: Erosion rates versus fraction of incised landscape within the catchments, equation is the best linear fit of the *incised* and *relict* catchments samples. C: Ratio between measured and calculated erosion rates against drainage area of the catchments.

2.4.3. Channel and hillslopes adjustment to the incision wave

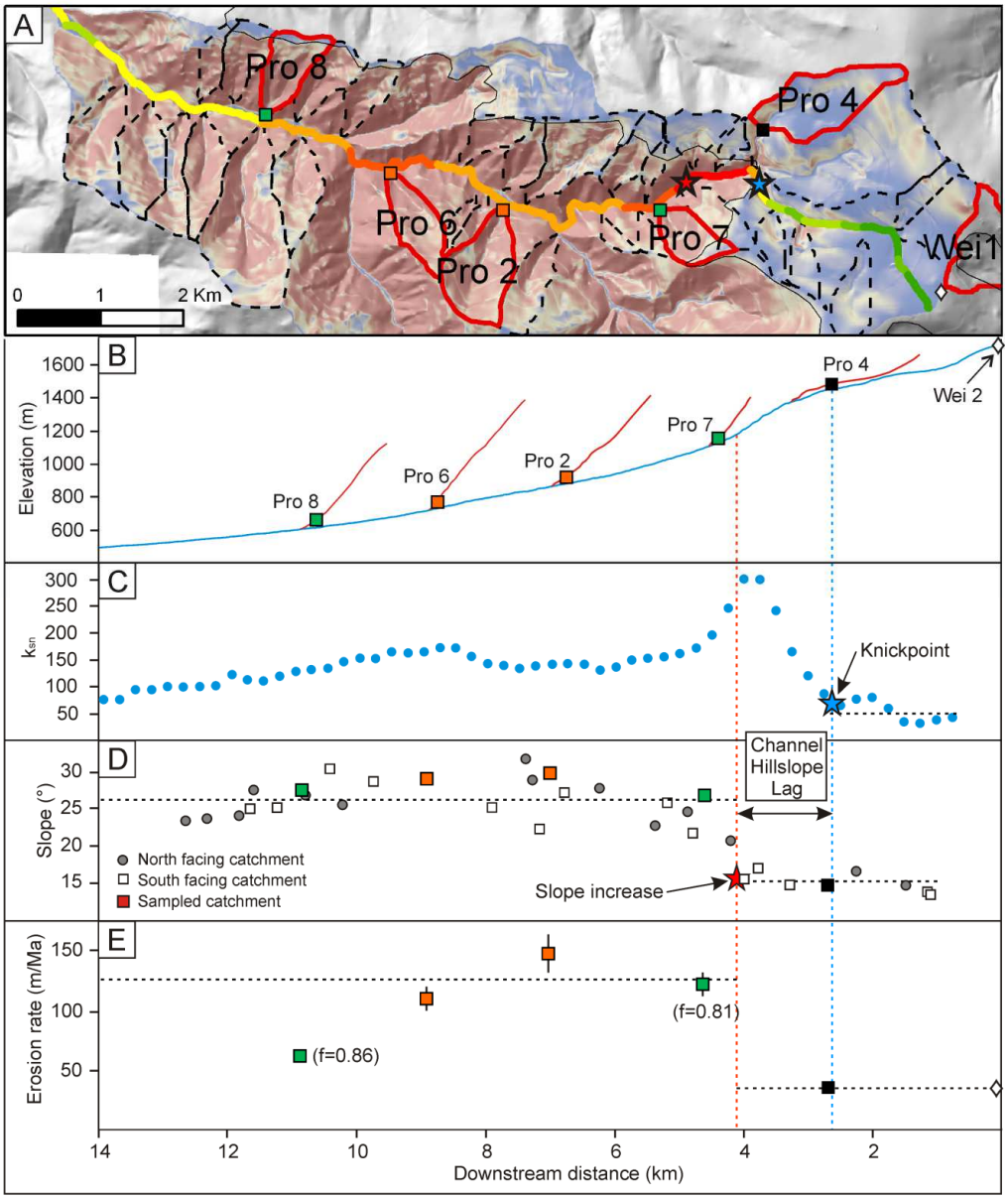

Figure 2.6: Map and along-stream variation of morphology and erosion rates of the Prössingbach River. A: Map of the catchment with the sampled basins, color coding for the slope gradient is from blue to red, for the channel the color coding is from green to red color coded with k_{sn}, mean slope of dashed black catchments is plotted in Fig. 2.6D. B: Channel profile of the Prössingbach River and sampled tributaries. C: Along stream variation of k_{sn} for the Prössingbach River calculated with a reference concavity of 0.45 and along 500 m long segments. D: Along stream variation of mean slope of tributaries catchments. E: Along stream variation of erosion rate of the sampled tributaries catchments, *f* is fraction of incised landscape for the *mixed* samples, dashed black lines are average erosion rate of *incised* (Pro-2, Pro-6) and *relict* (Pro-4, Wei-2) samples for the two parts of the landscape.

The Prössingbach catchment, located North West of the Koralpe summit, is the most incised of the Koralpe large catchments (Fig. 2.2). It is therefore a good area to investigate how channel, hillslopes and erosion rates adjust to the incision wave. The channel profile of the

Prössingbach River shows a clear separation between the upper relict landscape and the lower incised landscape separated by a prominent knickpoint (Fig. 2.6A, B, C). Interestingly the mean slope of small tributary catchments connected to the Prössingbach River shows a sharp increase 1.5 km downstream of the knickpoint (Fig. 2.6A, D). The lag between the knickpoint and the increase in slope of adjacent hillslopes can be explained by the time needed for the hillslopes to propagate the incision signal upstream and increase the mean slope of the catchment. The erosion rate shows a good correlation with the mean slope of the catchments. The two *relict* erosion rates are very low (36 m/Ma) and the two *incised* catchment show higher erosion rate (average of 130 m/Ma) (Fig. 2.5E). As explained earlier, the *mixed hillslope* catchments Pro-8 and Pro-7 are interpreted as random values between the two erosion rate signals and are therefore not taken into account for interpretations.

The time response of hillslopes can be estimated by the distance between the knickpoint and the location downstream where the hillslopes have propagated the erosion signal up to the crest: the shorter the distance, the faster the time response (Hurst et al., 2012). For the Prössingbach catchment, this would suggest that the hillslopes time response for this catchment is different between the North facing hillslopes and the South facing hillslopes. Indeed, the sample Pro-8 is located 9 km downstream of the knickpoint and the incision have not yet propagated until the crest while hillslopes located south of the Prössingbach River are entirely incised only ~ 3 km downstream of the knickpoint (Fig 2.6A). However, the geometry of the fluvial network of this catchment, with the larger tributaries joining the Prössingbach River from the South (Fig. 2.2), could also explain the difference between North facing and South facing catchments.

2.4.4. Calculation of incision timing and total relative base level fall for the Koralpe Mountain

The difference in erosion rates between the two parts of the Koralpe landscape clearly shows that the landscape is currently adjusting to a wave of incision. However, the cause of this incision is difficult to understand if the timing of the incision is not known. We use the measured ^{10}Be-derived erosion rates and the known amount of incision into the Koralpe relict landscape (Chapter 1) to calculate the incision timing (Δt_k) and the total relative base level fall (ΔB_k) with equation (2.1) and (2.2). Results of these calculations for the Koralpe Mountain yield an incision time (Δt_k) of 4.0 ± 1.0 Ma and a total relative base level fall (ΔB_k) of 543 ±

143 m since the beginning of the incision (Table 2.2). U_i and U_f are taken as the average erosion rate of the catchment from the relict landscape (49 ± 8 m/Ma) and the average erosion rate from the incised landscape catchments (137 ± 15 m/Ma) respectively (Table 2.1, 2.2). This timing of incision can be interpreted as the minimum age for the onset of incision because only the vertical incision is taken into account with equation (2.1) and (2.2). Lateral knickpoint migration is therefore neglected and the calculated time of incision could be shorter than the real onset of incision. However, for the Koralpe Mountain, this difference is likely to be minimal because knickpoint did not migrate for long horizontal distances (< 10 km, Fig., 2.2). The calculated timing of incision is therefore probably very close to the age of onset of incision into the relict landscape.

Table 2.2: Calculated time of incision and total relative base level fall

River name	Δz^a (m)	$\Delta t_k{}^b$ (Ma)	$\Delta B_k{}^c$ (m)
Waldensteinerbach	241 ± 22	2.7 ± 0.3	375 ± 23
Fallegbach	403 ± 67	4.6 ± 0.9	627 ± 69
Frassbach	216 ± 15	2.5 ± 0.3	336 ± 16
Schwarze Sulm	372 ± 76	4.2 ± 0.9	579 ± 79
Krennbach	480 ± 97	5.5 ± 1.2	747 ± 100
Feistritz	380 ± 56	4.3 ± 0.7	592 ± 58
	349 ± 92	**4.0 ± 1.0**	**543 ± 143**

a Amount of incision calculated from projection of six channels from Koralpe (Chapter 1)
b Time needed for the incision calculated as , with U_f and U_i being 137 ± 15 m/Ma and 49 ± 8 m/Ma respectively, see text for more details.
c Amount of total relative base level fall calculated as with U_i = 49 ± 8 m/Ma.

Although very simple, the calculations of Δt_k and ΔB_k with equation (2.1) and (2.2) are based on an important assumption. Indeed, ^{10}Be derived erosion rate from Koralpe are averaged on the last 4 -17 ka, the integration time of this method, but the calculated value for Δt_k is 4 ± 1 Ma. The calculation is therefore based on an extrapolation in time of the short term ^{10}Be-derived erosion rates from 4-17 ka to the last 4 Ma for both the erosion rate of the incised and relict landscape. This assumption appears very problematic because climate did change significantly and repeatedly in the last million years and the erosion rates from Koralpe may have changed to due to changes in precipitation for example. However, a good support to this assumption comes from the comparison between short-term erosion from Koralpe incised landscape and long-term incision rate of the Mur River in the Styrian Karst averaged over the last 4 Ma (Wagner et al., 2010). Wagner et al., 2010 interpreted a detailed incision history of the Mur River for the last 4 Ma but we are only interested here in the long-term record of incision rate. We therefore only use the mean incision rate of 130 ± 9 m/Ma calculated by Wagner et al., 2010, based on the highest and oldest dated sample (Fig. 2.6, sample DH4: 4.05

± 0.28 Ma; Wagner et al., 2010). The very good match between the ^{10}Be-derived erosion rate of the Koralpe incised landscape (137 ± 15 m/Ma) and the long term incision rate of the Mur River (130 ± 9 m/Ma, Wagner et al., 2010) strongly supports the assumption that the present day erosion rate of Koralpe are representative of the long-term timescale erosion rates (Fig 2.8). Thus, the calculation of Δt_k and ΔB_k with equation (2.1) and (2.2) appears robust despite the extrapolation in time of short-term ^{10}Be-derived erosion rates.

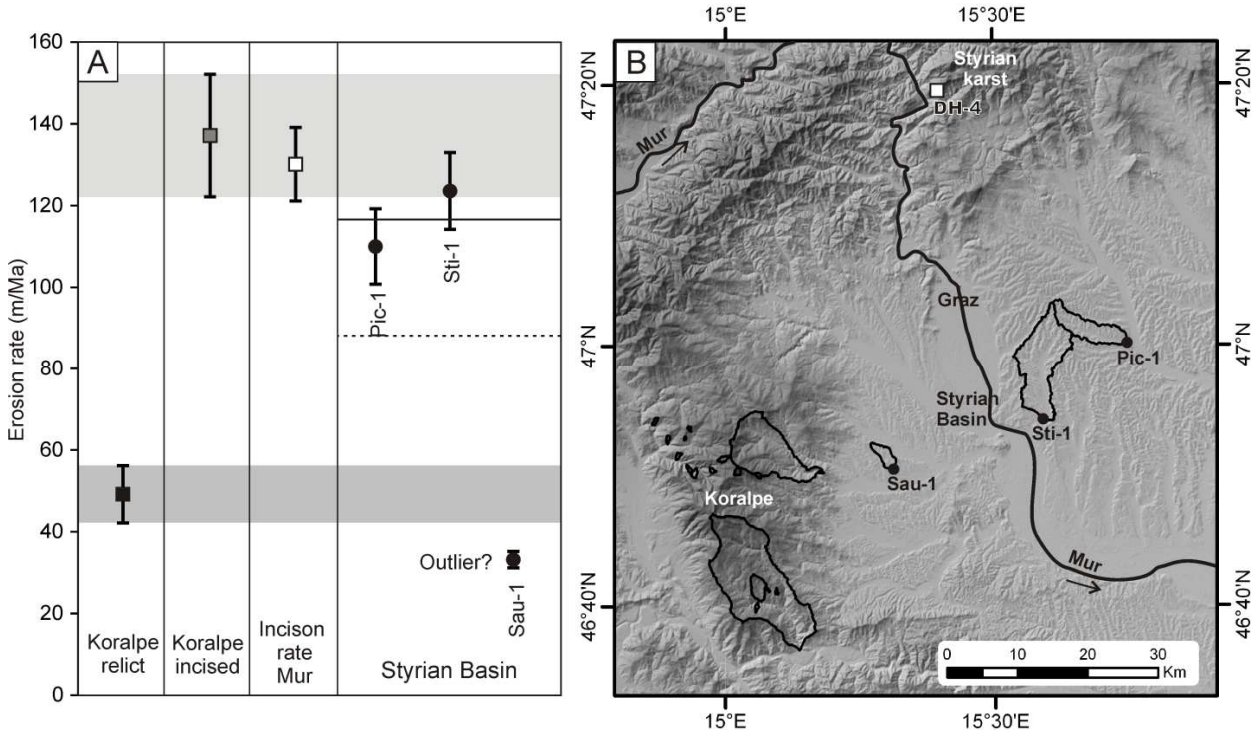

Figure 2.7: Comparison between short-term ^{10}Be-derived erosion rates from the Koralpe Mountain, the Styrian Basin and inferred long term incision rate of the Mur River in the Styrian Karst (Wagner et al. 2010), calculated as the average incision rate for the last 4 Ma. A: Lower and upper grey areas represent the average erosion rate of the Koralpe relict and incised landscapes respectively, with standard deviation around the mean. B: Location of the three Styrian Basin ^{10}Be samples and cave sample DH4 (Wagner et al., 2010).

2.5. Discussion

We compare the incision timing and total relative base level fall calculated for Koralpe with published data from regions in the vicinity of the Koralpe Mountain: the first dataset is a record of the incision rate of the Mur River calculated from cosmogenic burial age dating of cave sediments (Wagner et al., 2010, see above); the other two datasets consists in subsidence records of wells from the Styrian Basin (Ebner and Sachsenhofer, 1995; Sachsenhofer et al., 1998) and from the North Molasse Basin (Genser et al., 2007). For Koralpe, we have

calculated a total relative base level fall of 543 ± 143 m. There is a very good match between ΔB_k (543 ± 143 m), ΔB_c (525 ± 5 m), ΔB_{bs} (442 ± 103) and ΔB_{bn} (538 ± 170) (Fig. 2.7). The match between these four independent datasets suggests that the whole area may have responded at approximately the same time (between 6 Ma and 4 Ma) to an increase in rock uplift rate with a total relative base level fall of ~ 500 m since then (Fig. 2.7). Fig. 2.9 shows the spatial distribution of the amount of rock uplift for the different wells.

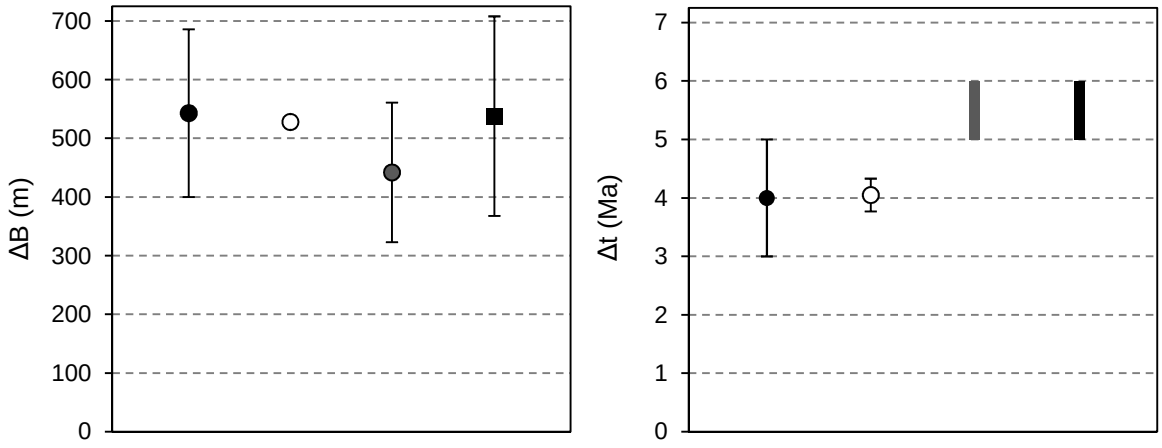

Figure 2.8: Comparison between total relative base level fall (ΔB) and time for the incision (Δt) from Koralpe, the Styrian Karst and the Styrian Basin. Black dots refer to Koralpe: ΔB_k and Δt_k (this study); white dots refer to the Styrian Karst: ΔB_c and Δt_c calculated from sample DH4 (Wagner et al., 2010; see text for more details); grey dot and grey bar refer to the Styrian Basin: ΔB_{bs} and Δt_{bs} (calculated from wells: *Ubersbach 1, Radkersburg 2, Pichla 1, Somat 1,* Ebner and Sachsenhofer, 1995; Sachsenhofer et al., 1998). Black square and black bar refer to the North Molasse Basin: ΔB_{bn} and Δt_{bn} (calculated from wells: *Strh 1, Stkr 1, Fü 3, Mlbg 1, Stbg 1, Li 1, Di 1, St 1, He 3,* Genser et al., 2007).

The erosion rates from the Styrian Basin also support this interpretation of a common uplift rock uplift history for a broad area. Indeed, two of the three calculated ^{10}Be-derived erosion rates from the Styrian Basin (Pic-1 and Sti-1) are very close to the erosion rate of the Koralpe incised landscape and the long-term incision rate into the Styrian Karst (Fig. 2.7). The sample Sau-1 yields a surprisingly low erosion rate maybe due to the small size of this catchment compared to the other two, and to its significantly lower mean slope. Thus, this small catchment may be not representative of the long-term erosion rate of the Styrian Basin and could be considered as an outlier. Even if we take in account the small Sau-1 catchment, the average erosion rate of the Styrian basin (88 ± 40 m/Ma) is significantly higher than the erosion rate of the Koralpe relict landscape 49 ± 7 m/Ma.

The two large catchments Pic-1 and Sti-1 average 117 m/Ma and match with the mean erosion rate of the Koralpe incised landscape (137 ± 15 m/Ma, Fig 2.7). This match support the view

that the Styrian Basin is currently responding to a relative base level fall that is transmitted to the Koralpe Mountain but has not yet reached the Koralpe relict landscape. Indeed, the similar erosion rates between the Styrian Basin and the Koralpe incised landscape suggest that both areas are responding to the same rock uplift rate (Fig. 2.1; $U_f = U_b$). It further suggests that practically all rock uplift rate is converted in erosion for the Styrian Basin (almost no surface uplift). In this context the basins elevation remains approximately constant at the level of the regional base level (Fig. 2.1).

2.5.1. Post-Miocene rock uplift increase in the Eastern Alps

Several possibilities have been proposed to explain the post-Miocene erosion increase in the European Alps (Dunkl et al., 2005; Wagner et al., 2010, Hergarten et al., 2010; Willett, 2010, Khulemann et al. 2002). At the eastern end of the Alps, a climate-related post-Miocene uplift driver seems very unlikely because the Koralpe region was relatively far from the main LGM ice body, which limits the post-LGM rebound due ice unloading to approximately 100 m (Sternai et al., 2012). Moreover, our calculated timing of increase in rock uplift of 4 ± 1 Ma is significantly older than the onset of periodic glaciations at ~ 2.5 Ma. Thus, the recent increase in uplift of the Koralpe Mountain documented here neither fits with the timing nor with the spatial occurrence of the last periodic glaciations in the Alps. It seems also clear that the incision is not the response to a more erosive climate and dissection of a plateau without vertical movements. Indeed, the incision seems closely related to the tectonic inversion from subsidence to uplift of the Styrian and North Molasse Basin which is necessarily related to an increase in rock uplift rate.

A simple explanation for this post-orogenic tectonic related increase in rock uplift could be the ongoing slow convergence (~2 mm/y) between Adria and stable Europe measured from GPS measurements (Bus et al., 2009). However, in this context, the North Molasse Basin should subside due to plate loading and not be uplifted as pointed out by Genser et al., 2007. We can therefore exclude a direct link between the convergence between Adria and Europe and the post-Miocene uplift of the eastern end of the Alps and surrounding sedimentary basins. If uplift related to climate and to active convergence can be excluded, a deep-seated process seems to be the only possibility to explain the observed increase in rock uplift rate since the late Miocene. Genser et al. (2007) suggested that slab break-off or delamination of the

European lithosphere underneath the Alps may have occurred at the end of the Miocene and lead to the observed uplift of the whole area. Fig. 2.8B shows the spatial variations in vertical movements and the location of the Adriatic slab at depth (Luth et al., 2013). The observed lower amount of uplift for the wells located in the eastern part of the North Molasse Basin could be explained by their larger distance to the Adriatic slab (Fig. 2.8B).

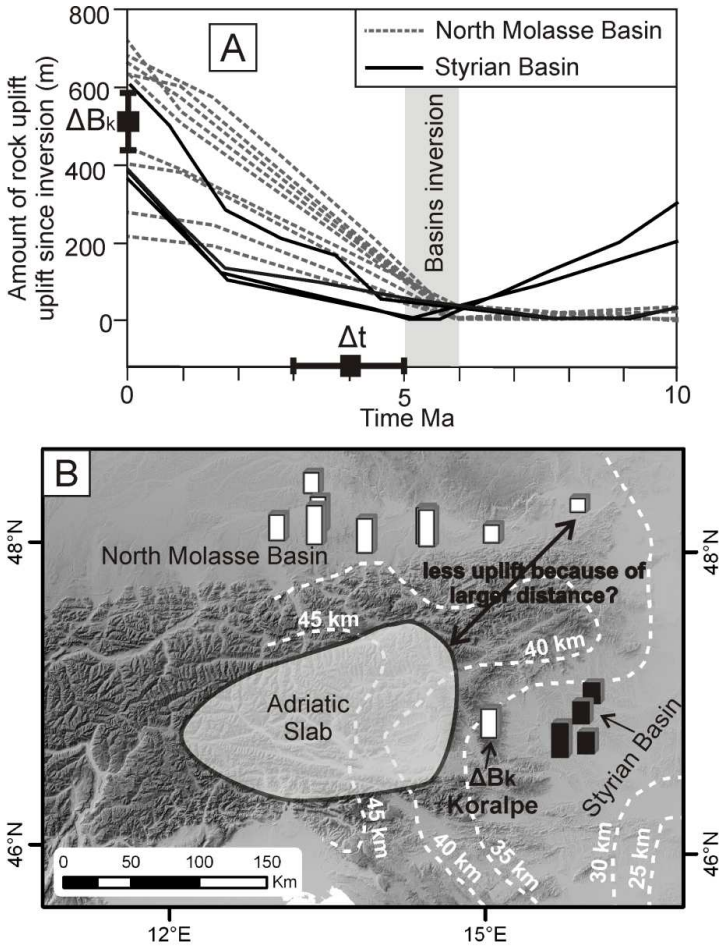

Figure 2.9: A: Comparison between total amount of base level fall calculated for Koralpe and amount of rock uplift since inversion of basin (Ebner and Sachsenhofer, 1995; Sachsenhofer et al., 1998; Genser et al., 2007, see Fig 2.6 for name of the wells), Δt refers to Δt_k . B: Adriatic slab extent at depth of 135 to 165 km (Luth et al., 2013), dashed white lines are Moho depth contour lines (Brückl et al., 2010).

2.5.2. Comparison between the Koralpe Mountain and the rest of the Alps

^{10}Be-derived erosion rate are from the Koralpe Mountain are approximately one order of magnitude lower than erosion rate from glaciated region of the Alps. Such difference could be explained by efficient glacial pre-conditioning of the glaciated Alps leading to sustained transient erosion, with higher erosion rate in heavily glaciated areas during LGM than in never glaciated setting (Norton et al., 2010a). However, taking in account the large distance

between our study area and other glaciated areas where ^{10}Be-derived erosion rate have been measured, the large difference in erosion rates may also be due to a very low erodibility of the high grade metamorphic rocks of the Koralpe, a differences in climate or in rock uplift rate. More data is therefore needed from a region ideally with different setting in pre-glacial erosion conditioning and with same climate and lithology, which make such hypothesis probably difficult to test in the Alps.

Our calculation of Δt_k and the amount of incision Δz can also give some rough estimate of the topographic evolution of the Koralpe Mountain since the late Miocene. The present-day relief of Koralpe (R_f), between the summit and the elevation of the Styrian basin, is ~ 1800 m. By removing the amount of incision (Δz) to the present day relief, we calculate an initial relief (R_i) of ~ 1450 m (Fig. 2.1). This simple calculation suggests that approximately 80 % of Koralpe relief was present before the increase in rock uplift rate and approximately 20 % was created by the incision after the rock uplift rate increase. If we assume a constant regional base level, the elevation of the Koralpe summit was around 1800 m elevation compared to its present-day elevation of 2140m. Although this suggests that most of the topography of Koralpe was present before 4 Ma, the increase of relief of 20% since then is significant.

At the scale of the Alps, such amount of surface uplift (350 m) seems very modest compared to the present-day topography of the Alps, with many summits well above 4000 m elevation. For example, if the surface uplift that we have documented here occurred with the same magnitude in other places of the Alps, the increase of summit elevation would only be of 10 % for a summit with 3500 m initial elevation, which is fairly common in all regions of the glaciated Alps. However, our results are of interest for the entire Alps because if this tectonic related rock uplift increase occurred in some of the glaciated Alps it could have contributed to create feedback mechanism between the small amplitude tectonic related uplift documented here and the well constrained climate related uplift. Thus, although modest in term of amplitude (350 m) the documented tectonic related uplift could be an explanation for the "missing uplift" in the glaciated Alps because of potential positive feedback mechanism with climate-related increase in erosion and uplift (Norton et al., 2010a; Sternai et al., 2012).

2.6. Conclusion

- ^{10}Be-derived erosion rates from the never glaciated Koralpe Mountain are approximately one order of magnitude lower (36-149 m/Ma) than erosion rates from previously glaciated regions of the Alps.

- We interpret the erosion rates of small catchments comprising both relict and incised landscape as random values between two end members erosion signal because of poor sediment mixing in the channel at the sampling location. However, the erosion rates show a clear difference between incised and relict landscape and support the interpretation of the Koralpe Mountain as a transient landscape adjusting to a wave incision.

- The calculated onset of incision for the Koralpe Mountain is 4 ± 1 Ma and the amount of total relative base level fall is 543 ± 143 m. These results fit with datasets from surrounding regions (Styrian Karst, Styrian Basin and North Molasse Basin) and suggest a common rock uplift increase for the whole area at the end of the Miocene.

- At the eastern end of the Alps, the post-Miocene uplift driver is unlikely to be directly due to active convergence between Adria and Europe or the result of a climatic change. We suggest that the increase in rock uplift rate may be due to a deep-seated process such as delamination of the lithosphere below the Alps or a slab break-off.

Chapter 3

Overall conclusions

In this thesis I have presented a combined analysis of a particular landscape of the Alps. Indeed, the studied region, located at the eastern end of the Alps, largely escaped the last periodic glaciations and therefore displays a purely fluvial landscape up to 2000 m elevation. Such landscape is rare in the Alps and is particularly interesting to study long term landscape evolution based on morphometric analysis. Indeed, to date fluvial erosion is better understood than glacial erosion and simple relationship between drainage area and slope of rivers can be very successful to document recent incision and uplift history of a mountain. Here, I have used such a morphometric approach in combination with apatite AHe ages and cosmogenic ^{10}Be derived erosion rates. The combination of these three different methods allowed to better constrain the topographic evolution of the easternmost never glaciated part of the Alps, from the Early Miocene to the present.

The Koralpe and Pohorje mountains of the Eastern Alps show evidence of transient erosion based on morphometric parameters such as hillslopes gradient and channel profiles analysis. Their landscapes can be divided into an upper relict landscape, and lower incised landscape. The Koralpe and Pohorje relict landscapes are younger than 16-15 Ma as indicated by the exhumation of the Pohorje granite and the extent of the relict landscape on both sides of the tilted Koralpe block. This exclude the possibility that these relict landscapes represent older (Pre-Miocene) deformed relict landscapes. The Koralpe and Pohorje relict landscapes were most likely created during the late Miocene, between 16-15 Ma and 5 Ma, a period of tectonic quiescence that allowed the topography to decay and become smoother. The subsequent dissection of these two relict landscapes involved incision of 383 ± 105 m.

^{10}Be-derived erosion rates from the unglaciated Koralpe Mountain are 36-149 m/Ma and are approximately one order of magnitude lower than erosion rates from previously glaciated regions of the Alps. We interpret the erosion rates of small catchments comprising both relict and incised landscape as random values between two end members erosion signal because of poor sediment mixing in the channel at the sampling location. However, the erosion rates show a clear difference between incised and relict landscape and support the interpretation of the Koralpe Mountain as a transient landscape adjusting to a wave incision.

The calculated onset of incision for the Koralpe Mountain is 4 ± 1 Ma and the amount of total relative base level fall is estimated to be 543 ± 143 m. These results are consistent with datasets from surrounding regions (Styrian Karst, Styrian Basin and North Molasse Basin) and suggest a common rock uplift increase for the whole area at the end of the Miocene. At

the eastern end of the Alps, the post-Miocene uplift driver is unlikely to be directly due to active convergence between Adria and Europe or the result of a climatic change. The increase in rock uplift rate may be due to a deep-seated process such as delamination of the lithosphere below the Alps or a slab break-off. This hypothesis partly remains speculative and would merit further work, but importantly, climate can clearly be excluded as a driving mechanism for the uplift of the studied region of the Alps. Therefore, the results presented in this thesis are important because they show, for the first time in the European Alps, a tectonic control on fluvial landforms and present day erosion rate at the eastern end of the Alps.

Appendix

This appendix is a collection of abstract form different conferences where I participated either with posters or talks. The abstract are sorted from the oldest to the most recent contribution.

4D kinematics of the Neogene Eastern Alps: An ArcGis based analysis of horizontal and vertical kinematics

Wölfler, A., Legrain, N., Stüwe, K., Fritz H., 2009. Workshop on Alpine Geological Studies, Cogne, Italy.

Prior to the Neogene, the evolution of the Alps may be considered to have started with the final subduction of oceanic lithosphere and the onset of continent – continent collision. The enigmatic Augenstein landscape indicates that topography was low (Frisch et al. 1998). Rapid extension in the Pannonian basin allowed an open eastern boundary and much of the N-S convergence was compensated by east-west extension. Since the basin inversion in the east, a change from extension to a regime of compression caused rapid, tectonically driven uplift at the orogen margins. This change in the external boundary conditions can be used as a time marker against which changes in horizontal and vertical kinematics, including present day erosion rates of the orogen, can be evaluated. As part of the TOPO Alps project "4D kinematics of the Neogene Eastern Alps" we present a high resolution database on both, horizontal and vertical kinematics of the orogen. By using the natural-neighbour interpolation tool provided by the ESRI-ArcMap9.3 GIS software, we created maps with zircon- (ZFT) and apatite fission track (AFT) ages covering the Eastern Alps. The maps show patterns of relatively young ages (ZFT $\leq$ 20, AFT $\leq$ 15 Ma) in the Tauern Window, the Niedere Tauern and Pohorje Mountains, suggesting that these units underwent the strongest denudation in Middle Miocene times. These conclusions is supported by long mean AFT lengths ($\geq$ 13 µm) and accelerated exhumation rates calculated from samples with paired zircon and apatite fission track- and/or zircon and apatite (U-Th)/He ages. On the contrary areas with older zircon- and apatite fission track ages are characterized by a trend to shorter mean AFT lengths ($\leq$ 13µm) and relatively low exhumation rates. These areas to the East of the Tauern Window, namely the Gurktal block, the Kor- and Saualpe, exhibit remnants of paleosurfaces of unknown age. The evaluation of data on horizontal kinematics of major fault zones and sedimentary record of intramonane basins to the east of the Tauern Window suggests four different main deformation stages: (1) pre-Karpatian N to NW directed compression causing strike slip motion and large offset in km scale; (2) Badenian to Sarmation phase of extension

accompanied with the formation of intramontane basins; (3) Late Miocene E-W compression causing fault reactivation, basin inversion and uplift of distinct regions; (4) Pliocene to recent NW to N compression with mainly strike slip faulting, seismology and recent uplift patterns. While many of these details are known, an orogen-scale compilation and interpretation is still missing.

Active tectonics at the Eastern end of the Alps: The Alps are certainly not "dead" at all

Stüwe, K., Wagner, T., Wölfler, A., Legrain, N., 2009. Geophysical Research Abstracts 11, EGU2009-9332, EGU General Assembly, Vienna, Austria.

In the literature many contributions have recently claimed that: "the Alps are tectonically dead". Much of this work has followed the recognition that the central part of the Alps appears to have changed their tectonic regime since the Miocene and deformation has propagated into the foreland. The inactivity of the Central Alps comes to no surprise, as the geophysical community has long established that the (counter clockwise) rotation pole of the Adriatic plate relative to Europe is due south of the central Alps near Torino implying zero convergence in the Central Alps to north of it. Conversely, this rotation pole implies north-south extension in the western Alps and north-south convergence east of the rotation pole in the Eastern Alps. In the Eastern Alps, seismology, active tectonics and recent uplift patterns show indeed that this region is currently highly active. In this contribution we defend the tectonic activity in the Eastern Alps against a growing body of opinion that the Alps are tectonically dead. For this we present two aspects: First we summarize our preliminary studies from the past including (i) cosmogenic burial ages suggesting up to 700 m of surface uplift within the last 4 my (ii) U/He age suggesting massive exhumation within the last 10 my (iii) morphometric studies showing substantial uplift of fluvial terraces. Secondly, we present our working groups plan to tackle this subject within the current TOPO-ALPS initiative.

Mapping out Paleo-Landscapes in the Non-Glaciated Part of the Alps: More Evidence for Young Uplift of this Part of the Alps

Stüwe, K., Legrain, N., Hergarten, S., 2010. Geophysical Research Abstracts12, EGU2010-11297, EGU General Assembly, Vienna, Austria.

The easternmost part of the Alps (east of the Niedere Tauern region) is the only part of the orogen where glacial carving can be excluded as a landscape forming process as it was never ice covered during the glaciation periods. As a consequence, this region is the only part of the Alps where morphometric analysis can be used to map out pre-glacial landscapes and use their morphology to make chronological interpretations. In view of recent suggestions that the surface uplift of the Alps may be extremely young, such mapping (and associated geochronology) is extremely important to test these predictions. For example, Hergarten et al. (EGU2010) use numerical interpretations of digital elevation models to show that the Alps are – on average – less than 10 my old. Similarly, Wagner et al. (EGU 2010) show that the non-glaciated part of the Alps has experienced some 600 m of surface uplift in the last 4 my reflecting the re-birth of a Miocene landscape. In order to test such predictions, we have begun to map paleosurfaces in several regions across the non-glaciated parts of the Alps, in particular in the Fischbacher Tauern and the Koralpe regions. Both regions feature peaks above 2000 m elevation above valleys only about 500 m high. However, closer investigations show that this picture can be refined: The peaks actually appear to form summits of an undulating landscape with up to 1000 m relief. Below about 1000 – 1100 m surface elevation the landscape drops into steep gullies. We suggest that these gullies formed in the last 5 my, while the high landscape is possibly of Miocene age. Cosmogenic nuclei work is currently in progress to test these hypotheses.

Late Neogene denudation rates in the Eastern Alps as determined by low temperature thermochronology

Wölfler, A., Stüwe, K., Legrain, N., Fritz, H., 2010. Journal of Alpine Geology 52, Leoben, Austria.

Erosion affects the topographic form and kinematics of orogens, and it may provide dynamic feedbacks between climate and tectonics. Thermochronology measures the timing and rates at which rocks approach the surface and cool as a result of exhumation. Our study aims to better understand the Miocene to recent exhumation and erosion periods in the Eastern Alps. For this, we use a combination of zircon and apatite (U-Th)/He analysis, applied to rocks from both sides of the Penninic/Austroalpine boundary and by the evaluation of recently published low temperature thermochronological data. This approach allows monitoring the thermal history of exposed rocks in the temperature range between 300 to 40 °C, thus documenting exhumation from about 10 km crustal depth to near-surface levels.The Austroalpine units yield systematically older ages (zircon: 57.3 – 37.3 Ma; apatite: 14.7 – 9.1 Ma) than those from the Tauern Window (zircon: 18.6-13.5; apatite: 7.6 – 5.1 Ma) and both datasets display positive correlation with elevation. According to the age-elevation relationship and the assumption of a stable geothermal gradient of 25 °C/km we gain 0.2 mm/yr for the Austroalpine- and 0.7 for the Penninic units in middle to late Miocene times. The apatite (U-Th)/He data also provide indirect constraints on the average denudation rate for the time of closure of the cooling ages to present and yield 0.5 mm/yr for the Pliocene to recent. These values are comparable to those from the Central Alps where recent studies demonstrated that rock uplift is a response to climate-driven denudation. In the Eastern Alps however, a different geodynamic evolution must be considered. By evaluation of already published thermochronolgical data we can demonstrate that denudation in the eastern part of the Eastern Alps occurred at relatively low rates (in average: 0.1 – 0.2 mm/yr) during Miocene to recent times. The difference in denudation rates in the Tauern Window and the adjacent eastern crystalline units are considered to be related to distinct tectonic evolution and/or different lithospheric conditions beneath the eastern part of the Eastern Alps. The available geochronological data of the southeastern Tauern Window reveal episodes of accelerated cooling that coincide with denudation budget of the Eastern Alps. The increase in the sediment budget between 24 and 21 Ma is less pronounced by low temperature thermochronology. However this event is related to the buildup of topography and relief especially in the Swiss- and Western Alps as well as the western Eastern Alps, whereas

surface erosion and relief in the eastern Eastern Alps declined. Between 18 and 17 Ma a drastic increase of sediment discharge rates coincides with the ZFT data from the eastern Tauern Window. According to the lack of age-elevation relationships of the published ZFT data no estimation of exhumation rates is possible. However the ZFT data are consistent with a period or reorganization in the Eastern Alps. The new zircon helium data of our study fall exact in the time of decreasing sediment discharge between 16 and 14 Ma. Again a period of accelerated exhumation between 12 to 7 Ma is well documented by AFT and partly by AHe ages and may be correlated with the termination of E-W extension in the Eastern Alps.

Neogene denudation rates in the Eastern Alps as determined by low temperature thermochronology

Wölfler, A., Stüwe, K., Legrain, N., Fritz, H., 2011. Geophysical Research Abstracts 13, EGU2011-10101, EGU General Assembly, Vienna, Austria.

Erosion affects the topographic form and kinematics of orogens, and it may provide dynamic feedbacks between climate and tectonics. Thermochronology measures the timing and rates at which rocks approach the surface and cool as a result of exhumation. Our study aims to better understand the Miocene to recent exhumation and erosion periods in the Eastern Alps. For this, we use a combination of zircon and apatite (U-Th)/He analysis, applied to rocks from both sides of the Penninic/Austroalpine boundary and by the evaluation of recently published low temperature thermochronological data. This approach allows monitoring the thermal history of exposed rocks in the temperature range between 300 to 40 _C, thus documenting exhumation from about 10 km crustal depth to near-surface levels. The Austroalpine units yield systematically older ages (zircon: 57.3 – 37.3 Ma; apatite: 14.7 – 9.1 Ma) than those from the penninic Tauern Window (zircon: 18.6-13.5; apatite: 7.6 – 5.1 Ma) and both datasets display positive correlation with elevation. According to the age-elevation relationship gain 0.2 mm/yr for the Austroalpine- and 0.7 for the Penninic units in middle to late Miocene times. The apatite (U-Th)/He data also provide indirect constraints on the average denudation rate for the time of closure of the cooling ages to present and yield 0.5 mm/yr for the Pliocene to recent. These values are comparable to those from the Central Alps where recent studies demonstrated that rock uplift is a response to climate-driven denudation. In the Eastern Alps however, a different geodynamic evolution must be considered. By evaluation of already published thermochronolgical data we can demonstrate that denudation in the eastern part of the Eastern Alps occurred at relatively low rates (in average: 0.1 – 0.2 mm/yr) during Miocene times. The difference in denudation rates in the Tauern Window and the adjacent eastern crystalline units are considered to be related to distinct tectonic evolution and/or different lithospheric conditions beneath the eastern part of the Eastern Alps. The available geochronological data of the Tauern Window reveal episodes of accelerated cooling that coincide with the denudation budget of the Eastern Alps. An increase in the sediment budget between 24 and 21 Ma is less pronounced by low temperature thermochronology. However this event is related to the buildup of topography and relief especially in the Swiss- and Western Alps as well as the western Eastern Alps, whereas surface erosion and relief in the eastern Eastern Alps declined. Between 18 and 17 Ma a drastic increase of sediment discharge rates coincides with the zircon fission track data from the eastern Tauern Window. According

to the lack of age-elevation relationships of the published zircon fission track data no estimation of exhumation rates is possible. However the zircon fission track data are consistent with a period or reorganization in the Eastern Alps. The new zircon helium data of our study fall exact in the time of decreasing sediment discharge between 16 and 14 Ma. Again a period of accelerated exhumation between 12 to 7 Ma is well documented by apatite fission track and partly by apatite (U-Th)/He ages and may be correlated with the termination of E-W extension in the Eastern Alps.

New U-He ages for the Eastern Alps

Stüwe, K., Legrain, N., Wölfler, A., Dunkl, I., Ehlers, T., 2011. Geophysical Research Abstracts 13, EGU2011-8617, EGU General Assembly, Vienna, Austria.

With respect to the youngest part of the tectonic evolution of the Alpine orogen, the eastern end of the Alps holds a unique position. Firstly, this part of the orogen is the region with maximum convergence between the Adriatic and the European plates. This is due its position far east of the rotation pole of the Adriatic plate. Secondly, the eastern end of the Alps is the only region of the mountain belt where peaks exist that are substantially above 2000 m but have never been ice covered during the glaciation periods. As such, geomorphological evidence and low-temperature geochronology can be used to infer the young uplift history since the Miocene. Curiously, fission track ages are generally of Eocene or Oligocene age and are thus much older than in the remainder of the range. This contrast between active tectonism and old fission track ages suggest that the current tectonics, surface uplift and current erosion regime may be extremely young and separated from the Eocene exhumation by a substantial hiatus. U-He age dating is a method that allows to constrain the evolution during this hiatus. It measures cooling through about the 60◦C isotherm– a half way mark between fission track ages and surface temperature. Thus, it is a critical method to constrain if rocks cooled nearer the Oligocene exhumation as indicated by fission track ages or nearer to late Miocene – indicating the onset of the young tectonism. In this project we have aimed at a spatial coverage of the eastern Alps east of the Tauern window using U-He dating of apatite. Field work was done in summer 2010 and mineral separation and selection during late 2010. Our data are currently in analysis and will be presented during this meeting.

Large scale, small amplitude, post-Miocene surface uplift in the non-glaciated Eastern Alps: river profiles analysis and cosmogenic-derived ^{10}Be denudation rates

Legrain, N., Stüwe, K., Dixon, J.L., von Blanckenburg, F., Kubik, P., 2011. Geophysical Research Abstracts 13, EGU2011-10708, EGU General Assembly, Vienna, Austria.

In the ongoing debate about the increase in denudation rates around 5 Ma in the Alps and its possible causes and consequences on the topographic evolution of the orogen, the Eastern Alps is a far less studied area than the Swiss Alps. In this contribution, we present in-situ cosmogenic 10Be derived denudation rates from the Eastern end of the Alps, at the transition with the Pannonian Basin. This unglaciated region is in a different climatic and tectonic setting than the Swiss Alps and is still undergoing a moderate N-S convergence, providing the chance to isolate the influence of tectonically related uplift on erosion and landscape morphology. River profile analysis highlights a disequilibrium landscape across two unglaciated areas of the Eastern Austrian Alps (Koralpe and Fischbacher Alpen), that cannot be related to lithology or climate. A continuous 'relict landscape' exists in the upper portions of the two areas, which, is incised by several hundred meter deep gorges. Some rivers in these two areas have a sharp knickpoint separating the river profiles into their relict and actively incising parts. We use the calculated concavity and steepness indexes to project the relict river profile (upstream of the knickpoint) above the equilibrated lower section of the river. The total and active incision into the relict landscape is 100-200 m for Fischbacher Alpen and 250-350 m for Koralpe. This incision can be used as a proxy for the total amount of surface uplift of the relict landscapes relative to the surroundings. ^{10}Be derived denudation rates of 17 catchments across the region show clear differences between the relict and incising portions of the landscape. For Fischbacher Alpen, the denudation rates of the relict and incised landscapes are 94 m/Ma and 125 m/Ma respectively. Similarly, across Koralpe, the average denudation rate of the relict landscape is 55 _ 9 m/Ma, while catchments within the incised portion are 65-213 m/Ma and average 122 m/Ma. We observe a good positive linear correlation between the denudation rates and the normalized channel steepness index of the main channel at the confluence between the measured catchment and the main channel. These results suggest that the denudation rates of these small catchments (<2km^2) are primarily controlled by disparate rates of river incision across the region. Together, these data show a clear signal of tectonic uplift on both the landscape morphology and denudation rates. Based on previous studies, we infer that the incision and the surface uplift of the relict landscapes started at the end of Miocene (around 6-5 Ma) in response to the inversion of the Styrian

basin. However, the driver of this post-Miocene large scale small amplitude uplift (<500m) that affected the easternmost Alps, the Styrian Basin and the northern Molasse Basin remains unclear.

References

Auer, M., 2003. Regionalisierung von Schneeparametern—Eine Methode zur Darstellung von Schneeparametern im Relief. Universität Bern, 97 pp

Brown, R., Stallard, F., Larsen, M.C., Raisbeck, G.M., Yiou, F., 1995. Denudation rates determined from the accumulation of in-situ-produced 10Be in the Luquillo experimental forest, Puerto Rico, Earth Planet. Sci.Lett., 129, 193-202.

Brückl, E., Behm, M., Decker, K. Grad, M., Guterch, A., Keller, G.R., Thybo H., 2010. Crustal structure and active tectonics in the Eastern Alps, Tectonics, 29, doi: TC2011. 10.1029/2009TC002491.

Bierman, P.R., Steig, E.J., 1996. Estimating rates of denudation using cosmogenic isotope abundance in sediment, Earth Surf. Proc. Land. 21, 125–139.

Bus, Z., Grenerczy, G., Tóth, L., Mónus, P., 2009. Active crustal deformation in two seismogenic zones of the Pannonian region—GPS versus seismological observations, Tectonophysics, 474, 343–352.

Campani, M., Mulch, A., Kempf, O., Schlunegger, F., Mancktelow N., 2012. Miocene paleotopography of the Central Alps, Earth and Planetary Science Letters, 337–338, 174–185.

Carretier, S., Regard, V., Vassallo, R., Aguilar, G., Martinod, J., Riquelme, R., Pepin, E., Charrier, R., Herail, G., Farias, M., Guyot, J-L., Vargas, G., Lagane, C., 2012. Slope and climate variability control of erosion rates in the Andes of central Chile, Geology, doi:10.1130/G33735.1.

Cederbom, C.E., Sinclair, D.H., Schlunegger, F., Meinert, K.R., 2004. Climate-induced rebound and exhumation of the European Alps, Geology, 32, 709–712, doi: 10.1130/G20491.1.

Champagnac, J.D., Molnar, P., Anderson., R.S., Sue, C., Delacou, B., 2007. Quaternary erosion-induced isostatic rebound and exhumation of the European Alps, Geology, 35; 195-198, doi: 10.1130/G23053A.1.

Clark, M.K., Maheo, G., Saleeby, J., Farley, K.A., 2005. The non-equilibrium landscape of the southern Sierra Nevada, California, GSA Today, 15, doi: 10:1130/10525173(2005) 015<4:TNELOT>2.0.CO;2.

Clark, M.K., Royden, L.H., Whipple, K.X., Burchfiel, B.C., Zhang X., Tang, W., 2006. Use of a regional, relict landscape to measure vertical deformation of the eastern Tibetan Plateau, J. Geophys. Res., 111, F03002, doi: 10.1029/2005JF000294.

Delunel, R., van der Beek, P.A., Carcaillet, J., Bourles, D.L., Valla P.G., 2010. Frost-cracking control on catchment denudation rates: insights from in situ produced 10Be concentrations in stream sediments (Ecrins-Pelvoux massif, French Western Alps), Earth Planet Sci, Lett, 293, 72–83, doi:10.1016/j.epsl.2010.02.020.

DiBiase, R.A., Whipple K.X., Heimsath, A.M., Ouimet, W.B., 2009. Landscape form and millennial erosion rates in the San Gabriel Mountains, CA, Earth Planet. Sci. Lett., doi:10.1016/j.epsl.2009.10.036.

Dunai, T.J., 2000. Scaling factors for production rates of in situ produced cosmogenic nuclides: a critical reevaluation, Earth Planet. Sci. Lett., 176, 157–169.

Dunkl, I., Kuhlemann, J., Reinecker J., Frisch, W., 2005. Cenozoic relief evolution of the Eastern Alps — constraints from apatite fission track age-provenance of Neogene intramontane sediments, Austrian Journal of Earth Sciences, 98, 92–105.

Ebner, E., Sachsenhofer R.E., 1995. Paleogeography, subsidence and thermal history of the Neogene Styrian Basin (Pannonian basin system, Austria) in: Neubauer, E., Ebner, E., and Wallbrecher, E., (Editors), Tectonics of the Alpine-Carpathian-Pannonian Region, Tectonophysics, 242, 133-150.

Ehlers, T. A., Farley K. A., 2003. Apatite (U-Th)/He thermochronometry: methods and applications to problems in tectonic and surface processes, Earth and Planetary Science Letters, 206, 1-14.

Exner, C., 1976. Die geologische Position der Magmatite des periadriatischen Lineamentes. Verh. Geol. B.-A., 1976/2:3-64.

Flint, J. J., 1974, Stream gradient as a function of order, magnitude, and discharge, Wat. Resources Res., 10, 969–973.

Fodor, L., Gerdes, A., Dunkl, I., Koroknai, B., Pecskay, Z., Trajanova, M., Horvath, P., Vrabec, M., Jelen, B., Balogh, K., Frisch, W., 2008. Miocene emplacement and rapid cooling of the Pohorje pluton at the Alpine-Pannonian-Dinaridic junction, Slovenia, Swiss J. Geosci., 101, 255-271.

Frisch, W., Kuhlemann, J., Dunkl, I., Brügel, A., 1998. Palinpastic reconstruction and topographic evolution of the Eastern Alps during the late Tertiary extrusion, Tectonophysics, 297, 1-15.

Frisch, W., Dunkl, I., Kuhlemann, J., 2000. Post-collisional largescale extension in the Eastern Alps, Tectonophysics, 327, 239–265.

Genser, J., Cloetingh, S., Neubauer, F., 2007. Late orogenic rebound and oblique Alpine convergence: New constraints from subsidence analysis of the Austrian Molasse basin, Global Plan. Change, 58, 214–223.

Granger, D.E., Kirchner, J.W., Finkel, R., 1996. Spatially averaged long-term erosion rates measured from in situ-produced cosmogenic nuclides in alluvial sediment, J. Geol., 104, 249–257.

Hack, J.T., 1973. Stream-profile analysis and stream-gradient index, J. Res. U.S. Geol. Survey, 1, 421–429.

Hejl, E., 1997. “Cold spots” during the Cenozoic evolution of the Eastern Alps: thermochronological interpretation of apatite fission-track data, Tectonophysics, 272, 159–173.

Hergarten, S., Wagner, T., Stüwe K., 2010. Age and prematurity of the Alps derived from topography, Earth Planet. Sci. Let., 297, 453–460.

Hirt, C., Filmer, M. S., Featherstone, W. E., 2010. Comparison and validation of the recent freely available ASTER-GDEM ver1, SRTM ver4.1 and GEODATA DEM-9S ver3 digital elevation models over Australia, Australian J. Earth Sci., 57, 337-347.

Hurst, M.D., Mudd, S.M., Walcott, R., Attal, M., Yoo, K., 2012. Using hilltop curvature to derive the spatial distribution of erosion rates, J. Geophys. Res., 117, F02017, doi:10.1029/2011JF002057.

Kirby, E., Whipple, K.X., 2012. Expression of active tectonics in erosional landscapes, Journal of Structural Geology, 44, 54-75.

Kuhlemann, J., Frisch, W., Szekely, B., Dunkl, I., Kazmer, M., 2002. Postcollisional sediment budget history of the Alps: tectonic versus climatic control. Int J Earth Sci (Geologische Rundschau) 91:818–837.

Kurz, W.,Wölfler, A., Rabitsch, R., Genser, J., 2011. Polyphase movement on the Lavanttal Fault Zone (Eastern Alps): reconciling the evidence from different geochronological indicators, Swiss J. Geosci., 104, 323–343, DOI 10.1007/s00015-011-0068-y.

Luth S., Willingshofer, E., Sokoutis, D., Cloetingh, S., 2013. Does subduction polarity changes below the Alps? Inferences from analogue modelling, Tectonophysics, 582, 140-161, http://dx.doi.org/10.1016/j.tecto.2012.09.028.

McDowell, F. W., McIntosh, W. C., Farley, K. A., 2005. A precise 40Ar-39Ar reference age for the Durango apatite (U-Th)/He and fission-track dating standard, Chem. Geol. 214, 249-263.

Miller, S.R., Sakb, P.B., Kirby, E., Bierman P.R., 2013. Neogene rejuvenation of central Appalachian topography: Evidence for differential rock uplift from stream profiles and erosion rates, Earth and Planetary Science Letters 369–370, 1–12, http://dx.doi.org/10.1016/j.epsl.2013.04.007.

Montgomery, D., Brandon, M., 2002. Topographic controls on erosion rates in tectonically active mountain ranges, Earth and Planetary Science Letters, 201, 481–489.

Neubauer, F., Genser J., 1990. Architektur und Kinematik der östlichen Zentralalpen – eine Übersicht. Mitt. Naturwiss. Ver. Steiermark, 120, 203–219.

Norton, K.P., Abbühl, L.M., Schlunegger, F., 2010a. Glacial conditioning as an erosional driving force in the Central Alps, Geology, 38, 655–658, doi: 10.1130/G31102.1.

Norton, K.P., von Blanckenburg, F., Kubik, P.W., 2010b. Cosmogenic nuclide-derived rates of diffusive and episodic erosion in the glacially sculpted upper Rhone Valley, Swiss Alps. Earth Surf. Proc. Land., 35:651–662, doi:10.1002/esp.1961.

Norton, K.P., von Blanckenburg, F., DiBiase, R., Schlunegger, F., Kubik, P.W., 2011 Cosmogenic 10Be-derived denudation rates of the Eastern and Southern European Alps, Int. J. Earth Sci., 100,1163–1179, DOI 10.1007/s00531-010-0626-y4.

Ouimet, W.B., Whipple, K.X., Granger, D.E., 2009. Beyond threshold hillslopes: Channel adjustment to base-level fall in tectonically active mountain ranges, Geology, 37, 7, 579-582, doi: 10.1130/G30013A.1.

Persaud, M., Pfiffner, O. A., 2004. Active deformation in the eastern Swiss Alps: Post-glacial faults, seismicity and surface uplift: Tectonophysics, 385, 59–84, doi:10.1016/j.tecto.2004.04.020.

Pischinger, G., Kurz, W., Übleis, M., Egger, M., Fritz, H., Brosch, F. J., Stingl, K., 2008. Fault slip analysis in the Koralm Massif (Eastern Alps) and consequences for the final uplift of “cold spots” in Miocene times, Swiss Journal of Geosciences, 101, 235–254.

Ratschbacher, L., Frisch, W., Linzer, H.G., Merle, O. 1991. Lateral extrusion in the Eastern Alps, Part 2, Structural analysis, Tectonics, 10, 257–271.

Rantitsch, G., Pischinger, G., Kurz, W., 2009. Stream profile analysis of the Koralm Range (Eastern Alps), Swiss J. Geosc., 102, 31–41.

Reinecker, J., Lenhardt, W.A., 1999. Present-day stress field and deformation in eastern Austria, Int. Journ. Earth Sciences, 88, 532–550.

Reinhardt, L.J., Bishop, P., Hoey, T.B., Dempster, T.J., Sanderson, D.C.W., 2007. Quantification of the transient response to base-level fall in a small mountain catchment: Sierra Nevada, southern Spain, J. Geophys. Res., 112, F03S05, doi:10.1029/2006JF000524 .

Reischenbacher, D., Rifelj, H., Sachsenhofer, R. F., Jelen, B., Coric, S., Gross, M., Reichenbacher, B., 2007. Early Badenian Paleoenvironment in the Lavanttal Basin (Mühldorf Formation; Austria): Evidence from geochemistry and Paleontology, Austrian Journal of Earth Sciences, 100, 202–229.

Robl, J., Stüwe, K., 2005. Continental collision with finite indenter strength: 2. European Eastern Alps, Tectonics 24. doi:10.1029/2004TC001741.

Robl, J., Hergarten, S., Stüwe, K., 2008. Morphological analysis of the drainage system in the Eastern Alps, Tectonophysics, 460, 263–277.

Roering, J.J., Perron, J.T., Kirchner, J.W., 2007. Functional relationships between denudation and hillslope form and relief: Earth and Planetary Science Letters, v. 264, p. 245–258, doi:10.1016/j.epsl.2007.09.035.

Sachsenhofer, R. F., Lankreijer, A., Cloetingh, S., Ebner, F., 1997. Subsidence analysis and quantitative basin modeling in the Styrian basin (Pannonian Basin system, Austria), Tectonophysics, 272, 175–196.

Sachsenhofer, R. F., Dunkl, I., Hasenhüttl, C., Jelen, B., 1998. Miocene thermal history of the southwestern margin of the Styrian Basin: vitrinite reflectance and fission-track data from the Pohorje/Kozjak area (Slovenia), Tectonophysics, 297, 17–29.

Sachsenhofer, R. F., Jelen, B., Hasenhüttl, C., Dunkl, I., Rainer T., 2001. Thermal history of Tertiary basins in Slovenia (Alpine-Dinaride-Pannonian junction), Tectonophysics, 334, 77–99.

Schaller, M., von Blanckenburg, F., Hovius, N., Kubik, P.W., 2001. Large-scale erosion rates from in situ-produced cosmogenic nuclides in European river sediments, Earth Planet. Sci. Lett. 188, 441-458.

Schaller, M., von Blanckenburg, F., Veldkamp, A., Tebbens L.A., Hovius, N., Kubik, P.W., 2002. A 30,000 year record of erosion rates from cosmogenic ^{10}Be in Middle European river terraces, Earth Planet. Sci. Lett., 204, 307–320.

Schoenbohm, L. M., Whipple, K. X., Burchfiel, B. C, Chen, L., 2004. Geomorphic constraints on surface uplift, exhumation, and plateau growth in the Red River region, Yunnan Province, China, GSA Bull., 116, 895–909, doi: 10.1130/B25364.1.

Sölva, H., Stüwe, K., Strauss, P., 2005. The Drava River and the Pohorje Mountain Range (Slovenia): Geomorphological Interactions, Mitt. naturwiss. Ver. Steiermark, 134, 45–55.

Sternai, P., Herman, F., Champagnac, J. D., Fox, M. R., Salcher, B., Willett, S. D., 2012. Pre-glacial topography of the European Alps. Geology 40, 1067–1070 http://dx.doi.org/10.1130/G33540.1.

Strauss, P., Wagreich, M., Decker, K., Sachsenofer, R. F., 2001. Tectonics and sedimentation in the Fohnsdorf-Seckau Basin (Miocene, Austria): from a pull-apart basin to a half-graben, Int. J. Earth Science, 90, 549-559.

Tenczer, V., Stüwe, K., 2003. The metamorphic field gradient in the eclogite type locality, Koralpe region, Eastern Alps, Journal of Metamorphic Geology, 21, 4, 377–393.

Valla, P. G., Schuster, D. L., van der Beek, P., 2011. Significant increase in relief of the European Alps during mid-Pleistocene glaciations, Nature Geosci., 4, 688-692, doi:10.1038/ngeo1242.

van Husen, D., 1997. LGM and late-glacial fluctuations in the Eastern Alps, Quat. Int., 38/39, 109-118.

von Blanckenburg, F., 2006. The control mechanisms of erosion and weathering at basin scale from cosmogenic nuclides in river sediment, Earth Planet. Sci. Lett., 237, 462–479.

Wagner, T., Fabel, D., Fiebig, M., Häuselmann, P., Sahy, D., Xu, S.,Stüwe, K., 2010. Young uplift in the non-glaciated parts of the Eastern Alps, Earth Plan. Sci. Let., 295, 159–169.

Wagner, T., Fritz, H., Stüwe, K., Nestroy, O., Rodnight, H., Hellstrom, J., Benischke, R., 2011. Correlations of cave levels, stream terraces and planation surfaces along the River Mur—Timing of landscape evolution along the eastern margin of the Alps, Geomorphology, 295, 159–169, doi:10.1016/j.geomorph.2011.04.024.

Whipple, K.X., Tucker, G.E., 1999. Dynamics of the stream-power river incision model: implications for height limits of mountain ranges, landscape response timescales and research needs, J.Geophys.Res., 104, 17661–17674.

Whipple, K. X., Wobus, C., Crosby, B., Kirby, E., Sheehan, D., 2007. Stream profiler tool, www.geomorphtools.org.

Willenbring, J. K., von Blanckenburg, F., 2010. Long-term stability of global erosion rates and weathering during late-Cenozoic cooling, Nature, 465, 211-214, doi:10.1038/nature09044.

Willet, S. D., 2010. Late Neogene erosion of the Alps: a climate driver? An. Review Earth Plan. Sci., 38, 411–437.

Winkler-Hermaden, A., 1957. Geologisches Kräftespiel und Landformung, Springer Verlag, Vienna, 822 pp.

Wittmann, H., von Blanckenburg, F., Kruesmann, T., Norton, K.P., Kubik, P.W., 2007. Relation between rock uplift and denudation from cosmogenic nuclides in river sediment in the Central Alps of Switzerland, J. Geophys. Res., 112:F04010, doi:10.1029/2006JF000729.

Wolf, R. A., Farley, K. A., Kass, D. M., 1998. Modeling of the temperature sensitivity of the apatite (U-Th)/He thermochronometer, Chemical Geology, v. 148 pp. 105-114.

Wölfler, A., Kurz, W., Danisik, M., Rabitsch, R., 2010. Dating of fault zone activity by apatite fission track and apatite (U–Th)/He thermochronometry: a case study from the Lavanttal fault system (Eastern Alps), Terra Nova, 22, 274–282, doi: 10.1111/j.13653121.2010.00943.x.

Wölfler, A., Kurz, W., Fritz, H., Stüwe, K., 2011. Lateral extrusion in the Eastern Alps revisited: refining the model by thermochronological, sedimentary and seismic data. Tectonics, 30 TC4006, doi:10.1029/2010TC002782.

Wobus, C., Whipple, K.X., Kirby, E., Snyder, E., Johnson, J., Spyropolou, K., Crosby, B., Sheehan, D., 2006. Tectonics from topography: Procedures, promise, and pitfalls. In: Willett S.D., Hovius, N., Brandon, M.T., Fisher, D.M., (eds) Tectonics, climate, and landscape evolution: Geological Society of America Special Paper 398, Penrose Conference Series, Geological Society of America, pp 55–74

Acknowledgments

I would like to thank Kurt Stüwe for his good advice, his support throughout the years and for having giving me so much freedom in my work. I would also like to thank Chloé for the fieldwork, her support and patience during these years, and for pushing me to finish this thesis. The many discussions with Thomas Wagner were very constructive and helpful for this thesis. I also thank Harry Fritz for his good knowledge and expertise about the Eastern Alps.

I want to thank Friedhelm von Blanckenburg for having giving me the chance to work in his group for several months. I am grateful to Friedhelm, Jeannie Dixon, Hella Wittmann and "TB" Codilean for the many things I have learned about cosmogenic nuclides during my trips to the GFZ. I thank Julien Bouchez for his hospitality in Berlin.

I also want to thank Todd Ehlers and Eva Enkelmann for their many helps when I was in their lab in Tübingen picking apatite. Concerning apatites and many other topics I also want to thank Andreas Wölfler. I have to thank all my successive office mates for the good atmosphere during these years: Thomas, Emilie, Deta, Tamer, Angela. This work was funded by ESF/FWF Topo-Alps project (I152-N19).

Finally, I want to thank my parents and my family for the many help during these years.